# Early postmortem mapping of SARS-CoV-2 RNA in patients with COVID-19 and correlation to tissue damage

**Stefanie Deinhardt-Emmer[1]*, Daniel Wittschieber[2]*, Juliane Sanft[2], Sandra Kleemann[2], Stefan Elschner[2], Karoline F. Haupt[1], Vanessa Vau[1], Clio Häring[3], Jürgen Rödel[1], Andreas Henke[3], Christina Ehrhardt[3], Michael Bauer[4], Mike Philipp[5], Nikolaus Gaßler[6], Sandor Nietzsche[7], Bettina Löffler[1#], Gita Mall[2#]**

1 Institute of Medical Microbiology, Jena University Hospital, Am Klinikum 1, D-07747 Jena, Germany
2 Institute of Forensic Medicine, Jena University Hospital, Am Klinikum 1, D-07747 Jena, Germany
3 Section of Experimental Virology, Institute of Medical Microbiology, Jena University Hospital, Hans-Knöll-Str. 2, D-07745, Jena, Germany
4 Department of Anaesthesiology and Intensive Care Medicine, Jena University Hospital, Am Klinikum 1, D-07747 Jena, Germany
5 Department of Anaestesiology and Intensive Care Medicine, Greiz General Hospital, Wichmannstrasse 12, D-07973 Greiz, Germany
6 Section of Surgical Pathology, Institute of Forensic Medicine, Jena University Hospital, Am Klinikum 1, D-07747 Jena, Germany
7 Department of Electron microscopy, Jena University Hospital, Ziegelmühlenweg 1, 07743 Jena, Germany

* These authors share first authorship.
# These authors share last authorship.

Corresponding author:

Dr. Stefanie Deinhardt-Emmer
Institute of Medical Microbiology
Jena University Hospital
Am Klinikum 1
D-07747 Jena
Germany
Email: stefanie.deinhardt-emmer@med.uni-jena.de

**Abstract (193)**

Clinical observations indicate that COVID-19 is a systemic disease. An investigation of the viral distribution within the human body in correlation to tissue damage can help understanding the pathophysiology of SARS-CoV-2 infection.

We present a detailed mapping of viral RNA in 61 tissues and organs of 11 deceased patients with the diagnosis COVID-19. The autopsies were performed within the (very) early postmortem interval (mean: 5.6 hours) to avoid bias due to viral RNA and tissue degradation. Viral loads, blood levels of cytokines, prothrombotic factors as well as macro- and micro-morphology were correlated.

Very high (> $10^4$ copies/ml) viral loads were detected in the lungs of most patients and then correlated to severe tissue damage. Intact viral particles could be verified in the lung tissue by transmission electron microscopy. Viral loads in the lymph nodes were associated with a loss of follicular architecture. Viral RNA was detected throughout further extra-pulmonary tissues and organs without visible tissue damage. Inflammatory cytokines as well as the prothrombotic factors were elevated in all patients.

In conclusion, the dissemination of SARS-CoV-2-RNA throughout the body supports the hypothesis of a maladaptive host response with viremia and multi-organ dysfunction.

**Keywords:** SARS-CoV-2, COVID-19, early post-mortem interval, autopsy, transmission electron microscopy, histology

## Introduction

In December 2019, several cases of pneumonia caused by a novel *Betacoronavirus* called SARS-CoV-2 were first described in the city of Wuhan in China [1] and therefore named "coronavirus disease 2019" (COVID-19) [2]. Within a few months, the initially localized outbreak spread to countries all over the globe, being declared a pandemic [3]. At present, more than 8.5 million SARS-CoV-2 infections have been reported. The number of deaths attributed to COVID-19 has exceeded 450.000 worldwide [4].

COVID-19 occurs in varying degrees of severity. While approximately 81% of COVID-19 patients are experiencing mild symptoms, 14% suffer from respiratory distress [5]. The remaining 5% enter a critical condition with respiratory failure, endovascular complications, or multiple organ dysfunctions. Gastroenterological and neurological symptoms have been reported in case studies for 36.4% and 18.6% of COVID-19 patients, respectively [6,7]. The clinical observations suggest that COVID-19 is a systemic disease.

While marginal information is available about the regulation of SARS-CoV-2, Angiotensin-Converting Enzyme (ACE)2 and Transmembrane Protease Serine 2 (TMPRSS2), two membrane-bound proteins turned out to be crucial for the entry of the virus into cells [8,9]. ACE2 is not only expressed in epithelia of the lung but also in several other epithelia, endothelia, heart and renal tissues [10]. The viral replication and pathogenesis are widely unknown due to the lack of appropriate models [11]. One crucial step to elucidate the viral pathogenesis is the investigation of the distribution of the virus within the whole body.

In the present study, we (1) included full autopsies, (2) performed the autopsies in the (very) early post-mortem interval (1.5 – 15 h, mean: 5.6 h), (3) dissected organs and tissues without prior fixation in formalin, (4) measured SARS-CoV-2 RNA in an extraordinary high number of samples, (5) correlated viral load to tissue damage using comprehensive histopathological investigations, (6) visualized virus particles in the pulmonal tissue samples by means of transmission electron microscopy (TEM), and (7) determined post-mortem serum levels of inflammatory cytokines and prothrombotic factors. The so far unique feature of sampling in the (very) early post-mortem interval

was intended to provide reliable viral RNA (vRNA) measurements, enabled us to obtain blood serum, and provided well preserved tissue samples for ultrastructural analysis.

## Materials and Methods

*Autopsies and post-mortem sampling*

The study was approved by the local ethical board (registration no.: 2020-1773). Complete autopsies (inspection of cranial, thoracic and abdominal cavities plus dissection of all internal organs and their surrounding anatomical structures) of 11 patients with a SARS-CoV-2 infection (proven by naso-pharyngeal swab testing during hospitalization) and the clinical diagnosis of COVID-19 were included in this study. As soon as possible after death the closest relatives were contacted and gave their informed consent. Contrary to recommendations of the pathological professional societies not to perform autopsies earlier than 24 hours post-mortem and to store the organs in formalin before dissecting them, the autopsies in this study were performed 1.5 – 15 h (mean 5.6 hours) post-mortem and the organs were dissected directly without prior fixation. The same voluntary team including two experienced forensic pathologists conducted all autopsies considering all necessary precautions and using the comprehensive personal protective equipment as recommended by professional societies. The lungs, with high viral loads to be expected, were removed first and dissected last to avoid transfer of viral RNA to other organs/tissues. At each autopsy, a total of up to 61 native and non-fixed samples (5 locations of the nervous system, 14 of the respiratory tract with double sampling in the lungs, 10 of the cardiovascular system, 12 of the gastrointestinal tract, 3 of the urinary tract, 4 of the reproductive system, 2 of the endocrine system, 6 of the lymphatic system, 2 of hematological tissues and 3 samples of abdominal skin, abdominal subcutaneous tissue and of musculus psoas major) were collected after rinsing in clean tap water. Tissue samples were transferred to virological processing immediately after autopsy; blood samples were centrifuged to obtain serum. Samples of the same anatomical locations were fixed in 5% buffered formalin solution for comparative histopathological analysis and selected samples in glutaraldehyde for TEM.

*SARS-CoV-2 RNA detection*

All tissues were homogenized in RPMI-medium by using the FastPrep-24™ 5G Instrument (MP Biomedicals, Schwerte, Germany). Throw-away beads (Zymo Research Bashing Bead Lysis Tubes, Freiburg, Germany) were used to avoid contamination. After centrifugation (2 min, 12.000 rpm) supernatants were collected for the determination of the viral load. The RNA extraction was performed by using the QIAcube RNeasy Viral Mini Kit (Qiagen, Hilden, Germany) according to manufacturer`s guide. A qRT-PCR from RIDAgene (r-biopharm, Darmstadt, Germany) followed on Rotor-Gene Q (Qiagen, Hilden, Germany) in order to detect the E-gene of SARS-CoV-2. The RNA standard curve, prepared from the positive control of the RIDAgene (r-biopharm, Darmstadt, Germany) kit, was applied for quantification. The following scaling was applied: Very high (> $10^4$ copies/ml), high ($10^3$-$10^4$ copies/ml), moderate ($10^2$-$10^3$ copies/ml), low ($10^1$-$10^2$ copies/ml), and below detection limit (bdl).

*Detection of inflammatory and thrombotic parameters*

For the measurement of proinflammatory cytokines and coagulation parameters, a LEGENDplex™ Human Thrombosis Panel (13-plex) (BioLegend, San Diego, CA, USA) was used. 25 µl of the serum samples were transferred in duplicates into the 96-well filter plate and the LEGENDplex panel was performed following the manufacturer's instructions. The samples were measured the same day on a flow cytometer (BD, Accuri) and the protein amount was calculated by comparison to a standard curve. Serum samples of 5 healthy volunteers without any signs of infection were age-correlated and analyzed as control.

*Histopathological analysis*

After fixation for at least 24 h in 10% neutral buffered formalin, the tissue samples were dehydrated in a graded series of ethanol and xylene, mounted in paraffin and cut to 3 µm thick sections. In addition to hematoxylin eosin (HE) stains, other special stains such as EvG, Fe, PAS,

abPAS, Giemsa, Gomori Trichrome and Kongo Red were used following routine protocols. For immunohistochemistry the antibodies detailed in follow were used: AE1/3 (Dako/IR053), TTF-1 (Dako/IR056), CK7 (Dako/IR619), CK5/6 (Dako/IR780), p40 (Zytomed/MSK097), Ki67 (Dako/IR626), CD68 (Dako/M0876), CD61 (Dako/M0753), CD31 (Dako/IR610), CD34 (Dako/IR623), ASMA (Dako/IR611), CD3 (Dako/IR503), CD20 (Dako/IR604), MUM1 (Dako/IR644), Collagen IV (Dako/M0785), Tenascin (Chemicon/MAB19101). All immunostains were performed with the Dako Omnis immunostainer (Agilent) following routine procedures. The sections were examined microscopically (Axio Imager.M2, Carl Zeiss Microscopy GmbH), and representative photographs were taken (Axiocam 506 color, Carl Zeiss Microscopy GmbH; ZEN 2.6 (blue edition), Carl Zeiss Microscopy GmbH).

*Transmission electron microscopy*

During each autopsy several small pieces of lung tissue (2 mm cubes) were immediately fixed with freshly prepared modified Karnovsky fixative (4 % w/v paraformaldehyde, 2.5 % v/v glutaraldehyde in 0.1 M sodium cacodylate buffer pH 7.4) for 24 h at room temperature. After washing 3 times for 15 min each with 0.1 M sodium cacodylate buffer (pH 7.4) the tissue was further cut into 1 mm cubes and post-fixed with 2 % w/v osmiumtetroxide for 1 h at room temperature. During the following dehydration in ascending ethanol series post-staining with 1 % w/v uranylacetate was performed. Afterwards the samples were embedded in epoxy resin (Araldite) and sectioned using a Leica Ultracut S (Leica, Wetzlar, Germany). Based on the examination of semi thin sections regions of interest of approx. 500 µm x 500 µm in size were selected and trimmed. Finally, ultrathin sections were mounted on filmed Cu grids, post-stained with lead citrate, and studied in a transmission electron microscope (EM 900, Zeiss, Oberkochen, Germany) at 80 kV and magnifications of 3,000x to 50,000x. For image recording a 2K slow scan CCD camera (TRS, Moorenweis, Germany) was used.

## Results

*SARS-CoV-2 vRNA is detectable in various organs and tissues*

The investigation of COVID-19 patients included a full characterization of the clinical characteristics and parameters (Tab. 1). In detail, patients 1-7 received intensive care; patients 1-6 were mechanically ventilated; patient 7 was submitted to ECMO (extra-corporal membrane oxygenation); the patients 1-2 and 5-6 were treated with lopinavir/ritonavir. The patients 8-10 were not subjected to intensive care or ventilation according to their patients' provisions.

Our results show that patients 1-10 died of COVID-19, whereas patient 11 suffered from a metastasized squamous cell carcinoma of the cervix and died of an ileus following peritoneal carcinosis (Tab. 2 gives an overview of the macro- and micro-morphological autopsy findings). She had contracted COVID-19, received intensive care treatment but was not ventilated. Interestingly, autopsy detected previously undiagnosed malignancies in patients 2 (chronic lymphatic leukemia, CLL) and 10 (endometrial carcinoma). In addition, patient 6 had an incidentaloma of the thyroid gland.

The determination of the E-gene of SARS-CoV-2 by using qRT-PCR detected a mean of very high to high viral loads in the lungs of all patients (Fig. 1a). Patients 1-10 showed very high titers, reaching up to $10^7$ RNA copies/ml (Fig. 1b). High to moderate to low viral loads were detected in further structures of the respiratory tract, such as mesopharynx, epiglottis and trachea in patients 1-8. In patient 10 with a non-COVID-19-associated cause of death, vRNA could only be detected in moderate to low amounts in the trachea.

Patients 1-10 also showed variable (very high to very low) viral loads in at least 2 samples of the lymphatic system. Lymphatic structures with topological relation to the respiratory tract were always positive for vRNA.

Of the patients with intensive care treatment (patients 1-7), patients 1, 3, 4 and 5 exhibited moderate to very low viral loads in the cardiac samples (Fig. 1c). Patients 2, 6 and 7 exhibited no

vRNA in the heart muscle. The vascular samples showed overall higher viral loads in more patients than the cardiac samples.

Viral RNA could not be detected in the blood except for the patients 3-5. The patients 1, 2, 6 and 7 who were treated with lopinavir/ritonavir were tested negative for the blood. Viral RNA was present in the bone marrow of all 3 patients who tested positive for the blood but also in further 3 patients who tested negative for the blood.

Patients 3-5 had vRNA in variable amounts throughout the small and large intestine. Patients 6 and 7 tested negative for all 12 gastrointestinal samples. Patient 9 is noticeable as almost all gastrointestinal samples exhibit moderate to very high viral loads.

Viral RNA could be detected in endocrine organs, in the urinary tract and in the reproductive organs as well. Only the patients 3-5 were tested positive for the central nervous system. Skin (abdominal), subcutaneous tissue (abdominal) and skeletal muscle (psoas major) tested negative in all patients.

Due to the very early post-mortem interval in which the autopsies were performed, we were able to verify the vRNA findings with TEM of a lung sample of patient 3 by detecting intact SARS-CoV-2 viral particles within a lung fibrocyte (Fig. 2).

*Proinflammatory and prothrombotic parameters*

To analyze the proinflammatory response of the 11 patients, we measured Interleukin (IL)-6 (Fig. 3a) and IL-8 (Fig. 3b) postmortem. Both parameters showed significantly elevated serum levels in all cases compared to control levels of 5 healthy volunteers.

Since abnormalities in the coagulation system was described for COVID-19 patients[12], we analyzed the prothrombotic parameters of the blood of the deceased patients. The disseminated intravascular coagulation was described previously and one suggested role of coagulation is to limit the infection dissemination[13]. Additionally, it is discussed that coagulation processes cause hyper-inflammatory responses in viral infection[14].

Our results show significantly higher serum levels of tissue plasminogen activator (tPa) (Fig. 3c) of COVID-19 patients compared to healthy volunteers. P-Selectin (Fig. 3d), a cell adhesion molecule of platelets necessary for the recruitment of platelets and the binding process to the endothelium[15], was measured in serum levels significantly higher than the controls in all patients. D-Dimer-serum levels (Fig. 3e) were partly elevated in patients. However, no significant elevation could be found. The plasminogen activator inhibitor (PAI, Fig. 3f), an important inhibitor of tPa[16], was significantly elevated in the blood serum of all patients.

A biomarker for potential cardiovascular risk stratification sCD40L (Fig. 3g) was significantly elevated in all patients. Further, the coagulation Factor IX (Fig. 3h) was measured at significantly elevated levels in the blood serum of all patients as well. It is discussed to function as a mediator between viruses and cells[17]. The P-Selektin Glykoprotein Ligand-1 (PSGL-1) could be determined as not significantly higher than the values within the healthy volunteer group.

*Macro- and micro-morphologic findings*

Macroscopic signs of severe and extensive lung damage were found in all patients. In patients 1, 3-5, 9 and 10, the lungs with prominent hyperemia and edema displayed a fragility of the tissue (Fig. 4a, b). In contrast, the lungs of patients 6-8 displayed a firmer and more consolidated pattern with only some aspects of edema and hyperemia (Fig. 4c-e). In the lung of patient 3, a nodular demarcated damage was found which correlated with a fungal superinfection (Fig. 4f). Patients 6, 9 and 10 had a purulent bronchitis and bronchopneumonia due to a bacterial superinfection, but patient 9 exhibited a severe pharyngitis.

Several features of coagulopathies were found including infarction of the lung (Fig. 4g) and the spleen (Fig. 4h) as well as fulminant thromboses of the periprostatic venous plexus (Fig. 4i) and hemorrhage of the cerebellum (Fig. 4j). Vascular stasis and fibrinous thrombi were present in patients 1-2 and 8-10. Thrombemboli were found in patients 2, 4, 5 and 10 to a variable extent. In patient 2 pulmonary embolisms were fatal.

Microscopically, lung tissues in patients 1, 3-5, 9 and 10 revealed changes similar to the early (exudative) phase of diffuse alveolar damage (DAD). The consistent acute changes included strong intraalveolar and interstitial hemorrhages (Fig. 5a, Fig 5b), architectural injuries with a diffuse alveolar damage pattern (such as hyaline membranes, fibrinous edema and interstitial proliferation), sporadic signs of cellular inflammation (mostly lymphocytes and few plasma cells) and severe loss of structured pneumocytes. Frequently, cells with enlarged cytoplasm and big nuclei were found admixed with multinucleated giant cells and features of squamous metaplasia and pattern of bronchiolization (Fig. 5a, b, c). Enlarged alveolar cells were detached from the alveolar wall (Fig. 5d). The clusters of enlarged cells were strongly positive for AE1/3 (Fig. 5e), but only few cells were co-labeled for TTF1 (Fig. 5f). Lung histology in patients 6-8 displayed a pattern similar to the later (proliferative) phase of diffuse alveolar damage (DAD). Giant cells and cell aggregates resembling squamous metaplasia were frequently found and sometimes accompanied by fibroblastic proliferations (Fig. 5g, h).

While the upper lobes of the lung of patient 2 showed only moderate emphysema (Fig. 6a), the hemorrhagic tissue damage was restricted to the middle and lower lobes of the right and the lower lobe of left lung (Fig. 6b). Vasculitis-like features were observed in patients 2, 3, 4, 8 and 9 with sporadic mild lympho-plasma cellular infiltrates around pulmonary artery branches (Fig. 6c, d). However, in patient 7 a strong lymphocyte-dominant intra-alveolar infiltrate was found (Fig. 6e, f). In particular, megakaryocytes were sometimes detectable in alveolar capillaries (Fig. 6g, h).

A common histological feature in all patients was a loss of follicular architecture in the lymph nodes with architectural changes (Fig. 7a). In the bone marrow of patient 9, the highest viral loads were found, and significant hemophagocytosis was detectable by microscopy (Fig. 7b). Interestingly, the correlation of high viral load and tissue damage as seen for the lung was not found in cardiac or aortic tissues. The cardiac tissues showed sometimes pre-existing changes (fibrosis and chronic ischemic damage), but neither severe damage nor inflammation or necrosis of cardiomyocytes were found (Fig. 7c). Sometimes an increased cellularity in the otherwise unremarkable cardiac tissue was

seen (e.g. in patient 1), suggestive for an activated cardio-mesenchyme (Fig. 7d). The large vessels were unremarkable as well. Figure 6e demonstrates a section of the thoracic aorta of patient 5 from the same anatomical location as the sample that tested highly positive for vRNA. Neither the intima (asterisk) nor the upper tunica media displayed any inflammatory cells or tissue damage. In the colon mucosa strong signs of epithelial damage were not visible using light-microscopy (e.g. patient 3; Fig. 7g), and the histology of the pancreas was well preserved (e.g. patient 9; Fig. 7h).

## Discussion

In clinical practice, many critically ill COVID-19 patients show multiple organ involvement apart from lung failure, in particular vascular dysfunction, such as thrombosis and/or impaired microcirculation [18]. A dysregulated immune response was observed starting with a phase of immuno-suppression followed by a proinflammatory phase up to a cytokine storm [19]. The cytokine storm might play an important role and supports the hypothesis that COVID-19 could have a strong immunopathological component.

Regarding viral pathogenesis and toxicity of the novel SARS-CoV-2, some aspects are known based on previous studies with SARS-CoV [20]. The virus can infect nasal mucous cells, pneumocytes and alveolar macrophages. ACE2 is the main receptor for the cellular binding process [11]. Since the ACE2 receptor is expressed not only by cells in the respiratory system [21] it is reasonable to assume, that other organ systems can also be targeted by SARS-CoV-2.

Quite a few morphological studies have been published so far. Some are single case reports based on necropsies of lung, liver and heart[22], partial autopsies of the thoracic cavity[23] or full autopsies[24]. Some represent small (n = 2–3) case series based on surgical lung resectates[25] or on full autopsies[26-29]. The larger case studies (n = 7-21) focus on single organs like the lungs[30], the spleen[31], the kidneys[32] or heart and lungs[33,34] or report comprehensive organ findings obtained by minimally invasive sampling[35] or full autopsies[36-39]. Only few of the aforementioned autopsy studies report viral loads in selected organs and tissues[27,32,36,38]. The post-mortem interval between death and autopsy was

over 48 h[40], 11-84.5 h[36], 1-5 d[38], 4 d (on average with a maximum of 12 d)[39]. The sample size of our case series can be compared to the larger autopsy case series from literature. Edler et al.[39] report the gross results of 80 autopsies from a still larger case series, but present histological investigations of the first 12 cases only. To our knowledge, the present study is the only one so far that focused on keeping the post-mortem interval as small as possible to avoid bias due to degradation of SARS-CoV-2 virus particles, SARS-CoV-2 RNA and tissue ultrastructure. Regarding vRNA degradation, the values reported by Puelles et al.[32] show comparatively low viral loads among their cases, even in the lungs as primary target of SARS-CoV-2. Wichmann et al.[38] reported the highest values in the lungs with 1.2 x $10^4$ to 9 x $10^9$ copies/ml, while our highest values reached up to $10^7$ vRNA copies/ml. To our knowledge, the present study is also the only one so far that measured viral loads in a wide variety of organs and tissues by taking and processing 61 samples per patient. The importance of multiple sampling within one organ is emphasized by the results of patient 10 (Fig. 1b), where only 2 of on the whole 7 samples from the heart were positive. If only one sample had been taken, the viral loads could have been false negative. Based on the mapping of SARS-CoV-2 RNA throughout the whole human body, we were able to correlate viral loads in many organs and tissues to macro- and micromorphology. So far, TEM has been applied to the lung samples only to verify the presence of intact virus particles.

We detected the highest viral loads and the most severe tissue damage in the lungs. The lung samples of all patients showed large cells, sometimes multinucleated giant cells, similar to giant cells described in cases of a respiratory syncytial virus (RSV) infection. The preliminary immuno-staining pattern of the enlarged cells indicated that they represent affected pneumocytes. Squamous (metaplastic) large cells and clusters of giant cells are reported by most morphological studies, except for one[30]. Our remaining findings in the lung samples agree very well with the findings of the other work groups, especially with data by Nunes Duarte-Neto et al.[35]. The strict topological correlation of viral loads and histopathological damage is emphasized by the results in patient 2. The samples from the upper lung lobes showed normal unremarkable tissue (Fig. 6a) corresponding to negative viral

loads, while the samples from the lower lung lobes revealed severe tissue damage corresponding to high and moderate viral loads (Fig. 6b).

All patients who died due to COVID-19 (patients 1-10) had viral RNA in at least some samples of the lymphatic tissue. Lymphatic tissue with topological relation to the respiratory tract (e.g. tonsils, cervical lymph nodes, hilar lymph nodes) was overall more positive than lymphatic tissue without such topological relation (e.g. mesenteric lymph nodes, spleen, appendix). One remarkable finding in the lymph node samples of all patients was the loss of follicular structure (Fig. 7a). An atrophy of lymphatic tissue has been described for the SARS-CoV infection by Gu et al. [41] and discussed as a crucial determinant of disease outcome by Perlman and Dandekar[42]. The spleen was positive in patients 1, 3, 4, 5 and 9 who presented with the micro-morphology of early lung damage and negative in the patients 6, 7, 8 and 10 who presented with the micro-morphology of later lung damage or did not die of COVID-19-pneumonia (patient 2). A further interpretation of viral loads in the appendix is futile since the appendix showed age-related and chronic pathologic changes accompanied by a loss of lymphatic tissue.

Viral loads in the cardiac tissue were moderate to very low and systematically (all samples) detected in the patients with early lung damage, while patients with later lung damage displayed viral loads only sporadically or not at all. The cardiac histology of the left ventricle, anterior wall, basal part of patient 1 with moderate viral load is presented in Fig. 7c, d. Except for an activation of mesenchymal cells, which needs further investigation, the histology was unremarkable. In accord with Buja et al.[33] we also found a pericarditis in patient 1 and multifocal acute injury of cardiomyocytes which is frequently observed in critically ill patients under catecholamine therapy.

The viral loads in the samples from the vascular tissue (aorta and pulmonary artery) followed a similar distribution pattern depending on the stage of lung damage but were higher compared to the cardiac tissue. The unremarkable histology of the thoracic aorta of patient 5 with a high viral load is presented in Fig. 7e, f. The conclusion by Varga et al.[29] that SARS-CoV-2 induces an endothelitis cannot be comprehended.

The viral loads in the gastrointestinal tract were variable. The very high viral loads in patient 9 throughout the upper gastrointestinal tract as well as in the small and large bowels appear noticeable. The histology of the corresponding tissue samples was unremarkable. According to the clinical documentation, patient 9 did not exhibit any gastrointestinal symptoms.

Viral RNA could also be detected in low to very high amounts in the samples from the endocrine organs, the urinary tract, the nervous system, and the reproductive system. Interestingly, the samples of the patients 1, 2, 6 and 7 who were treated with lopinavir/ritonavir were tested negative.

The same distribution pattern among the patients was observed regarding the viral RNA in the blood. Apart from the patients 8-11 who were not under intensive care (patients 8-10) or did not die of COVID-19 (patient 11), it is noticeable that among the patients receiving intensive care prior to death (patients 1-7) only the patients 3, 4 and 5 were tested positive for the blood, while the patients 1, 2, 6 and 7 tested negative. The latter patients were treated with lopinavir/ritonavir, so that an effect of antiviral medication on preventing viremia may be suggested.

The patients with viral RNA in the blood also showed viral RNA in the bone marrow. The patients 1, 8 and 9 were negative in the blood but positive in the bone marrow. Patient 9 showed by far the highest viral loads in the bone marrow. Histology of the bone marrow apart from hypercellularity, left shift and an increased number of megakarocytes showed a significant amount of hemophagocytosis (Fig. 6b). Hemophagocyosis is a morphological feature of the makrophage activation syndrome (MAS) or the hemophagocytic lymphohistiocytosis (HLH)[43,44]. The clinical characteristics of COVID-19, including very high ferritin levels and very high proinflammatory interleukins, resemble MAS and HLH[45] and have already encouraged therapeutically attempts[46].Further studies are needed in order to clarify this aspect.

To further elucidate the immunological host response, we measured interleukin 6 and interleukin 8 in the postmortem serum samples. The serum levels of interleukin 6 were significantly

387 elevated in all patients including patient 11 who died of multiple organ failure following an ileus. The
388 serum levels of interleukin 8 were significantly elevated as well.

389 In accordance with other autopsy studies[38,40] we observed thrombo-embolic events in 4 of the
390 11 patients. Patients 2 died of pulmonary embolism and patient 4 suffered multiple lung and spleen
391 infarctions due to venous thromboses. The patients 5 and 10 presented with sporadic emboli in the
392 lung histology. In conjunction with a general impairment of microcirculation, histologically visible as
393 homogenous eosinophilic sludge in the small arterioles, capillaries and venoles in multiple organ
394 samples from patients 1, 8 and 9, on the whole 7 (of 11) patients suffered hyper-coagulation. Some
395 studies hypothesize that SARS-CoV-2 can induce non-coordinated reactions between the coagulation
396 and fibrinolysis systems that result in hyper-coagulation and hemorrhage[18]. The measured pro-
397 thrombotic factors were almost all significantly elevated in all patients.

398 In sum, we presented an autopsy series of 11 patients with COVID-19. The autopsies were
399 performed in the (very) early postmortem interval to avoid bias due to degradation of vRNA, virus
400 particles, and tissue structures. SARS-CoV-2 RNA could be detected in very high to high amounts in
401 the lungs and in very high to very low amounts in the lymphatic tissue. TEM visualized SARS-CoV-2
402 particles in the lung tissue. Viral loads and histological tissue damage were strongly correlated in the
403 lungs even on the organ level (patient 2). Histological structure changes were also present in the
404 lymph nodes (atrophy and loss of follicles). Considerable viral loads were detected in many other
405 tissue samples from different extra-pulmonary organs and tissues without (light)microscopically
406 evident tissue damage.

407 In conclusion, SARS-CoV-2 may be able to infect different cell types in different organs and
408 tissues but may not be able to replicate in non-respiratory organs/tissues as efficiently as in the
409 respiratory ones. This hypothesis might explain the range from severe tissue damage with clear
410 cytopathic effects in lung tissue to the unremarkable histology of extra-pulmonary tissues despite
411 similar viral loads. Infected extra-pulmonary cells could nevertheless contribute to inflammation,
412 hyper-coagulation and multiple organ dysfunction.

**Acknowledgments**

We thank Jenny Pfeifer, Nico Möller, Cornelia Jacob and Christine Weiler with her fellow technicians for their excellent technical support.

**Conflict of Interest**

The authors declare no conflict of interest.

**Funding**

The authors acknowledge the support of this work by a grant from the IZKF (ACSP02). In addition, the project was funded by the Carl Zeiss Foundation.

# References


1 Zhu, N. *et al.* A Novel Coronavirus from Patients with Pneumonia in China, 2019. *N Engl J Med* **382**, 727-733, doi:10.1056/NEJMoa2001017 (2020).

2 Lu, R. *et al.* Genomic characterisation and epidemiology of 2019 novel coronavirus: implications for virus origins and receptor binding. *The Lancet* **395**, 565-574, doi:https://doi.org/10.1016/S0140-6736(20)30251-8 (2020).

3 El Zowalaty, M. E. & Järhult, J. D. From SARS to COVID-19: A previously unknown SARS- related coronavirus (SARS-CoV-2) of pandemic potential infecting humans - Call for a One Health approach. *One Health* **9**, 100124-100124, doi:10.1016/j.onehlt.2020.100124 (2020).

4 Dong, E., Du, H. & Gardner, L. An interactive web-based dashboard to track COVID-19 in real time. *The Lancet Infectious Diseases* **20**, 533-534, doi:https://doi.org/10.1016/S1473-3099(20)30120-1 (2020).

5 Wu, Z. & McGoogan, J. M. Characteristics of and Important Lessons From the Coronavirus Disease 2019 (COVID-19) Outbreak in China: Summary of a Report of 72 314 Cases From the Chinese Center for Disease Control and Prevention. *JAMA* **323**, 1239-1242, doi:10.1001/jama.2020.2648 (2020).

6 Pan, L. *et al.* Clinical Characteristics of COVID-19 Patients With Digestive Symptoms in Hubei, China: A Descriptive, Cross-Sectional, Multicenter Study. *The American journal of gastroenterology* **115**, 766-773, doi:10.14309/ajg.0000000000000620 (2020).

7 Mao, L. *et al.* Neurologic Manifestations of Hospitalized Patients With Coronavirus Disease 2019 in Wuhan, China. *JAMA Neurology*, doi:10.1001/jamaneurol.2020.1127 (2020).

8 Wang, Q. *et al.* Structural and Functional Basis of SARS-CoV-2 Entry by Using Human ACE2. *Cell*, doi:https://doi.org/10.1016/j.cell.2020.03.045 (2020).

9 Hoffmann, M. *et al.* SARS-CoV-2 Cell Entry Depends on ACE2 and TMPRSS2 and Is Blocked by a Clinically Proven Protease Inhibitor. *Cell* **181**, 271-280.e278, doi:10.1016/j.cell.2020.02.052 (2020).

10 Hamming, I. *et al.* Tissue distribution of ACE2 protein, the functional receptor for SARS coronavirus. A first step in understanding SARS pathogenesis. *The Journal of pathology* **203**, 631-637, doi:10.1002/path.1570 (2004).

11 Bar-On, Y. M., Flamholz, A., Phillips, R. & Milo, R. SARS-CoV-2 (COVID-19) by the numbers. *eLife* **9**, doi:10.7554/eLife.57309 (2020).

12 Connors, J. M. & Levy, J. H. COVID-19 and its implications for thrombosis and anticoagulation. *Blood* **135**, 2033-2040, doi:10.1182/blood.2020006000 (2020).

13 Antoniak, S. The coagulation system in host defense. *Research and Practice in Thrombosis and Haemostasis* **2**, 549-557, doi:10.1002/rth2.12109 (2018).

14 Yang, Y. & Tang, H. Aberrant coagulation causes a hyper-inflammatory response in severe influenza pneumonia. *Cell Mol Immunol* **13**, 432-442, doi:10.1038/cmi.2016.1 (2016).

15 Furie, B. & Furie, B. C. Role of platelet P-selectin and microparticle PSGL-1 in thrombus formation. *Trends in Molecular Medicine* **10**, 171-178, doi:10.1016/j.molmed.2004.02.008 (2004).

16 Cesari, M., Pahor, M. & Incalzi, R. A. Plasminogen activator inhibitor-1 (PAI-1): a key factor linking fibrinolysis and age-related subclinical and clinical conditions. *Cardiovasc Ther* **28**, e72-e91, doi:10.1111/j.1755-5922.2010.00171.x (2010).

17 Lenman, A. *et al.* Coagulation Factor IX Mediates Serotype-Specific Binding of Species A Adenoviruses to Host Cells. *Journal of virology* **85**, 13420, doi:10.1128/JVI.06088-11 (2011).

18 Ji, H.-L., Zhao, R., Matalon, S. & Matthay, M. A. Elevated Plasmin(ogen) as a Common Risk Factor for COVID-19 Susceptibility. *Physiological Reviews* **100**, 1065-1075, doi:10.1152/physrev.00013.2020 (2020).

19 Li, H. *et al.* SARS-CoV-2 and viral sepsis: observations and hypotheses. *Lancet*, S0140-6736(0120)30920-X, doi:10.1016/S0140-6736(20)30920-X (2020).

20 Qian, Z. *et al.* Innate immune response of human alveolar type II cells infected with severe acute respiratory syndrome-coronavirus. *American journal of respiratory cell and molecular biology* **48**, 742-748, doi:10.1165/rcmb.2012-0339OC (2013).

21 Jia, H. P. *et al.* ACE2 receptor expression and severe acute respiratory syndrome coronavirus infection depend on differentiation of human airway epithelia. *Journal of virology* **79**, 14614-14621, doi:10.1128/JVI.79.23.14614-14621.2005 (2005).

22 Xu, Z. *et al.* Pathological findings of COVID-19 associated with acute respiratory distress syndrome. *Lancet Respir Med* **8**, 420-422, doi:10.1016/S2213-2600(20)30076-X (2020).

23 Karami, P. *et al.* Mortality of a pregnant patient diagnosed with COVID-19: A case report with clinical, radiological, and histopathological findings. *Travel Med Infect Dis*, 101665, doi:10.1016/j.tmaid.2020.101665 (2020).

24 Aguiar, D., Lobrinus, J. A., Schibler, M., Fracasso, T. & Lardi, C. Inside the lungs of COVID-19 disease. *Int J Legal Med*, doi:10.1007/s00414-020-02318-9 (2020).

25 Tian, S. *et al.* Pulmonary Pathology of Early-Phase 2019 Novel Coronavirus (COVID-19) Pneumonia in Two Patients With Lung Cancer. *J Thorac Oncol* **15**, 700-704, doi:10.1016/j.jtho.2020.02.010 (2020).

26 Ding, Y. *et al.* The clinical pathology of severe acute respiratory syndrome (SARS): a report from China. *J Pathol* **200**, 282-289, doi:10.1002/path.1440 (2003).

27 Sekulic, M. *et al.* Molecular Detection of SARS-CoV-2 Infection in FFPE Samples and Histopathologic Findings in Fatal SARS-CoV-2 Cases. *Am J Clin Pathol*, doi:10.1093/ajcp/aqaa091 (2020).

28 Barton, L. M., Duval, E. J., Stroberg, E., Ghosh, S. & Mukhopadhyay, S. COVID-19 Autopsies, Oklahoma, USA. *Am J Clin Pathol* **153**, 725-733, doi:10.1093/ajcp/aqaa062 (2020).

29 Varga, Z. *et al.* Endothelial cell infection and endotheliitis in COVID-19. *Lancet* **395**, 1417-1418, doi:10.1016/S0140-6736(20)30937-5 (2020).

30 Ackermann, M. *et al.* Pulmonary Vascular Endothelialitis, Thrombosis, and Angiogenesis in Covid-19. *N Engl J Med*, doi:10.1056/NEJMoa2015432 (2020).

31 Xu, X. *et al.* [Pathological changes of the spleen in ten patients with new coronavirus infection by minimally invasive autopsies]. *Zhonghua Bing Li Xue Za Zhi* **49**, E014, doi:10.3760/cma.j.cn112151-20200401-00278 (2020).

32 Puelles, V. G. *et al.* Multiorgan and Renal Tropism of SARS-CoV-2. *N Engl J Med*, doi:10.1056/NEJMc2011400 (2020).

33 Buja, L. M. *et al.* The emerging spectrum of cardiopulmonary pathology of the coronavirus disease 2019 (COVID-19): Report of 3 autopsies from Houston, Texas, and review of autopsy findings from other United States cities. *Cardiovascular Pathology* **48**, 107233, doi:https://doi.org/10.1016/j.carpath.2020.107233 (2020).

34 Fox, S. E. *et al.* Pulmonary and cardiac pathology in African American patients with COVID-19: an autopsy series from New Orleans. *Lancet Respir Med*, doi:10.1016/S2213-2600(20)30243-5 (2020).

35 Nunes Duarte-Neto, A. *et al.* Pulmonary and systemic involvement of COVID-19 assessed by ultrasound-guided minimally invasive autopsy. *Histopathology*, doi:10.1111/his.14160 (2020).

36 Menter, T. *et al.* Post-mortem examination of COVID19 patients reveals diffuse alveolar damage with severe capillary congestion and variegated findings of lungs and other organs suggesting vascular dysfunction. *Histopathology*, doi:10.1111/his.14134 (2020).

37 Schaller, T. *et al.* Postmortem Examinations of Patients With COVID-19. *JAMA*, doi:10.1001/jama.2020.8907 (2020).

38 Wichmann, D. *et al.* Autopsy Findings and Venous Thromboembolism in Patients With COVID-19: A Prospective Cohort Study. *Ann Intern Med*, doi:10.7326/M20-2003 (2020).

39 Edler, C. *et al.* Dying with SARS-CoV-2 infection-an autopsy study of the first consecutive 80 cases in Hamburg, Germany. *Int J Legal Med*, doi:10.1007/s00414-020-02317-w (2020).

40 Lax, S. F. *et al.* Pulmonary Arterial Thrombosis in COVID-19 With Fatal Outcome: Results From a Prospective, Single-Center, Clinicopathologic Case Series. *Annals of Internal Medicine*, doi:10.7326/m20-2566 (2020).

41 Gu, J. *et al.* Multiple organ infection and the pathogenesis of SARS. *J Exp Med* **202**, 415-424, doi:10.1084/jem.20050828 (2005).

42 Perlman, S. & Dandekar, A. A. Immunopathogenesis of coronavirus infections: Implications for SARS. *Nat Rev Immunol* **5**, 917-927, doi:10.1038/nri1732 (2005).

43 Crayne, C. B., Albeituni, S., Nichols, K. E. & Cron, R. Q. The Immunology of Macrophage Activation Syndrome. *Front Immunol* **10**, doi:ARTN 119 10.3389/fimmu.2019.00119 (2019).

44 Al-Samkari, H. & Berliner, N. Hemophagocytic Lymphohistiocytosis. *Annu Rev Pathol-Mech* **13**, 27-49, doi:10.1146/annurev-pathol-020117-043625 (2018).

45 Colafrancesco, S., Alessandri, C., Conti, F. & Priori, R. COVID-19 gone bad: A new character in the spectrum of the hyperferritinemic syndrome? *Autoimmunity Reviews* **19**, 102573, doi:10.1016/j.autrev.2020.102573 (2020).

46 Dimopoulos, G. *et al.* Favorable Anakinra Responses in Severe Covid-19 Patients with Secondary Hemophagocytic Lymphohistiocytosis. *Cell Host & Microbe*, doi:10.1016/j.chom.2020.05.007 (2020).

# Early postmortem mapping of SARS-CoV-2 RNA in patients with COVID-19 and correlation to tissue damage

**Stefanie Deinhardt-Emmer[1]*, Daniel Wittschieber[2]*, Juliane Sanft[2], Sandra Kleemann[2], Stefan Elschner[2], Karoline F. Haupt[1], Vanessa Vau[1], Clio Häring[3], Jürgen Rödel[1], Andreas Henke[3], Christina Ehrhardt[3], Michael Bauer[4], Mike Philipp[5], Nikolaus Gaßler[6], Sandor Nietzsche[7], Bettina Löffler[1#], Gita Mall[2#]**

**Figure Legends:**

**Fig. 1a Overview of SARS-CoV-2 vRNA throughout the human body.** Postmortem determination of SARS-CoV-2 RNA with qRT-PCR of homogenized organs and tissues in copies/ml represented as decadic logarithm of 11 patients with mean value and standard deviation (SD) of the following systems: respiratory system, lymphatic system, gastrointestinal tract, urinary tract, nervous system, cardiovascular system, hematological tissues, reproductive system, and endocrine system. Intensity of colors describes the amount of RNA. Abbrev.: bdl (below detection limit), UL (upper lobe), ML (middle lobe), LL (lower lobe), LV (left ventricle), sr (suprarenal), VS (ventricular septum), RV (right ventricle), aw (anterior wall), pw (posterior wall), bp (basal part), ap (apical part), paraaort. (paraaortal). Figure was created by using Servier medical arts.

**Fig. 1b Individual vRNA load of the respiratory system, the lymphatic system, the cardiovascular system and hematological tissues.** Postmortem determination of SARS-CoV-2 RNA with qRT-PCR of homogenized organs and tissues in copies/ml represented as decadic logarithm of 11 patients. Abbrev.: bdl (below detection limit), UL (upper lobe), ML (middle lobe), LL (lower lobe), LV (left ventricle), sr (suprarenal), VS (ventricular septum), RV (right ventricle), aw (anterior wall), pw (posterior wall), bp (basal part), ap (apical part), nd (not determined), np (not present). Intensity of colors describes the amount of RNA.

**Fig. 1c Individual vRNA load of the gastrointestinal tract, the endocrine system, the urinary tract, the nervous system, and the reproductive system.** Postmortem determination of SARS-CoV-2 RNA with qRT-PCR of homogenized organs and tissues in copies/ml represented as decadic logarithm from patient 1-11. Abbrev.: bdl (below detection limit), nd (not determined), np (not present). Intensity of colors describes the amount of RNA.

**Fig.2 Transmission electron microscopic image of the lung tissue of patient 3.** (a) Alveolar septum showing intact capillaries with erythrocytes (asterisk) and the air space (cross). The blood-air barrier is damaged as the pneumocytes are missing and the basal membrane is exposed to air (arrowheads). (b-e) Close-ups of the 4 boxed regions in (a) from left to right

showing SARS-CoV-2 virus particles encased in plasmatic vesicles of alveolar fibrocytes. (f) Reference image of SARS-CoV-2 virus particles proliferated in cell culture (vero76).

**Fig. 3 Proinflammatory and prothrombotic factors.** Blood analysis of patient 1-11 by using Legendplex Panel (Biolegend, CA, USA) of the proinflammatory cytokines Interleukin (IL)-6 (a) and IL-8 (b) as well as tissue plasminogen activator (tPa) (c), P-Selectin (d), D-Dimer (e), Plasminogen activator inhibitor-1 (PAI) (f), soluble (s)CD40ligand(L) (g), Factor IX (h) and the P-selectin glycoprotein ligand 1 (PSGL-1) (i) in pg/ml compared to the mean of five controls (Control, healthy volunteers). Unpaired t-test, Mann-Whitney test $p<0.005$ ***; $p<0.05$ **; ns=not significant.

**Fig. 4 Macromorphology findings of COVID-19 patients.**

(a) Pneumonectomy of patient 1 showed strong congestion with liquids and hemorrhages. The tissue consistency was fragile.

(b) Cut surface of lung tissue in higher magnification as shown in (a). The pleura shows further hemorrhages.

(c) Pneumonectomy of patient 7 showed a more solid lung tissue without congestion. The tissue consistency was very firm.

(d) Cut surface of lung tissue in higher magnification as shown in (c). Lung tissue was retracted adjacent to the bronchus.

(e) Pale pleura visceralis of the lung of patient 6 with disseminated hemorrhages and signs of disturbed ventilation.

(f) Nodular transformation of lung tissue as phenomenon of fungal superinfection in patient 3.

(g) Hemorrhagic lung infarct in patient 4 due to a thrombembolus in a pulmonary artery branch.

(h) Anemic spleen infarct due to a clotted small artery in patient 4.

(i) Fulminant stasis and thromboses in the periprostatic plexus in patient 4.

(j) Cerebellar infarction (hemorrhagic) in patient 9.

**Fig. 5 Micromorphology lung findings of COVID-19 patients.**

(a) Destroyed lung tissue with intraalveolar hemorrhagia and aggregates of priominent epithelial cells resembling squamous metaplasia (patient 1; HE).

(b) Strong architectural damage of lung alveolar tissue with disruption of the epithelial barrier and intraalveolar accumulation of enlarged cells with prominent nuclei and visible nucleoli. Initial syncytial pattern is given (patient 2; HE).

(c) Lung tissues with multinucleated giant cells admixed with only few lymphocytes (patient 4; HE).

(d) Alveolar unit with band-like desquamation of the alveolar epithelial cells in the alveolar space partially filled with liquids, erythrocytes and few lymphocytes (patient 5; HE).

(e) Multinucleated giant cell in an alveolar space is strongly positive for keratins (patient 4; immunostaining AE1/3).

(f) Serial section of (e), the multinucleated giant cell after immunostaining against TTF1 (patient 4; immunostaining TTF1).

(g) Lung tissue with interstitial fibrosis (patient 8; EvG).

(h) Lung tissue with interstitial and intra-alveolar fibrosis (patient 8; EvG).

**Fig. 6 Micromorphology lung findings of COVID-19 patients.**

(a) Lung tissue with minimal emphysematic changes derived from the upper lobes without detectable viral loads (patient 2; HE).

(b) Severe hemorrhagic pneumonia in specimens from the lower lobes with high viral loads (patient 2; HE).

(c) Vasculitis-like changes around pulmonary artery branches (patient 4; HE).

(d) Damaged lung tissue with hemostasis and inflammatory changes adjacent to the pulmonary artery branch (patient 4; HE).

(e) Strong lymphocytic-predominant infiltration of lung tissues with hemorrhagia and interstitial edema (patient 7; HE).

(f) Higher magnification of the lymphocytic-predominant infiltrate (patient 7; HE).

(g) Lung tissue with a large nucleated cell in an alveolar capillary, suggestive for a megakaryocyte (arrow; patient 9; HE).

(h) The same tissue after immunostaining against CD61 (patient 9; immunostaining CD61).

**Fig. 7 Extra-pulmonary micromorphology findings of COVID-19 patients.**

(a) Overview of a mediastinal lymphnode with some nodular aggregates of lymphocytes, but destroyed lymphofollicular structures (patient 5; HE).

(b) Bone marrow with prominent hemophagocytosis (arrow) and maturating cells of the hematopoiesis (patient 9; HE).

(c) Myocardial tissue of the left ventricle (patient 1; HE).

(d) Myocardial tissue of the left ventricle in higher magnification with a minimal increase in cellularity indicating for an activated cardiomesenchyme (patient 1; HE).

(e) Thoracic aorta with a low number of non-inflammatory nucleated cells in an unsuspicious matrix (patient 5; HE).

(f) Tissue from the thoracic aorta in higher magnification. The endothelium is labeled with an asterisk (patient 5; HE).

(g) Colon mucosa with a crypt lined by goblet cells and enterocytes without any strong intraepithelial inflammation (patient 3; HE).

(h) Exocrine pancreas tissue with structural intact acini without inflammatory cells (patient 9; HE).

# Early postmortem mapping of SARS-CoV-2 RNA in patients with COVID-19 and correlation to tissue damage

## Figures

# Figure 1a

| Respiratory system | Mean | SD |
|---|---|---|
| Mesopharynx | 2.14 | 1.35 |
| Epiglottis | 2.75 | 1.93 |
| Trachea middle | 2.67 | 1.83 |
| Tracheal bifurcation | 3.73 | 2.39 |
| Right lung, UL | 3.99 | 2.42 |
| Right lung, ML | 4.02 | 2.04 |
| Right lung, LL | 4.29 | 2.42 |
| Left lung, UL | 4.10 | 1.98 |
| Left lung, LL | 2.06 | 1.78 |

| Lymphatic system | Mean | SD |
|---|---|---|
| Tonsilla palatina | 2.01 | 1.77 |
| Cervical lymph nodes | 2.51 | 1.42 |
| Hilar lymph nodes | 3.07 | 1.50 |
| Paraaort. lymph nodes | 1.59 | 1.58 |
| Spleen | 0.72 | 0.97 |
| Appendix vermiformis | 0.72 | 1.09 |

| Gastrointestinal tract | Mean | SD |
|---|---|---|
| Tongue | 1.66 | 1.53 |
| Gl. submandibularis | 0.94 | 0.82 |
| Oesophagus | 1.62 | 1.52 |
| Stomach, corpus | 0.91 | 1.87 |
| Duodenum | 0.88 | 1.54 |
| Jejunum | 1.00 | 1.45 |
| Pancreas | 0.24 | 0.59 |
| Liver | 0.76 | 0.98 |
| Gall bladder | 0.40 | 0.72 |
| Ileum | 1.34 | 1.86 |
| Colon | 1.03 | 1.83 |
| Rectum | 0.86 | 1.06 |

| Endocrine system | Mean | SD |
|---|---|---|
| Thyroid gland | 1.51 | 1.58 |
| Adrenal gland | 0.76 | 1.05 |

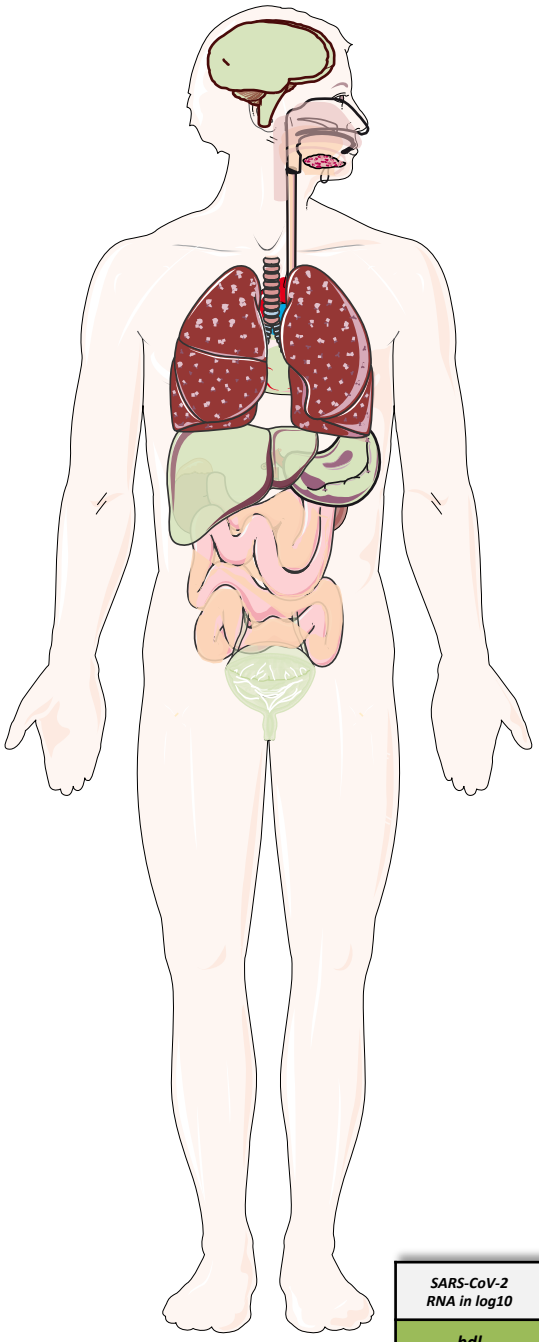

| *SARS-CoV-2 RNA in log10* |
|---|
| *bdl* |
| *0.01 – 0.99* |
| *1.00 – 1.99* |
| *2.00 – 2.99* |
| *3.00 – 3.99* |
| *from 4.00* |

| Nervous system | Mean | SD |
|---|---|---|
| Brain, frontal lobe | 0.40 | 0.79 |
| Brain, hippocampus | 0.39 | 0.68 |
| Cerebellum | 0.37 | 0.82 |
| Brain stem, pons | 0.69 | 1.31 |
| N. phrenicus | 0.56 | 1.03 |

| Cardiovascular system | Mean | SD |
|---|---|---|
| Aortic arch | 1.53 | 1.62 |
| Pulmonary artery | 2.69 | 2.05 |
| Abdominal aorta, sr | 1.22 | 1.27 |
| Heart, LV, aw, bp | 0.86 | 1.03 |
| Heart, LV, aw, ap | 0.77 | 0.88 |
| Heart, LV, pw, bp | 0.53 | 0.60 |
| Heart, LV, pw, ap | 0.74 | 0.85 |
| Heart, VS, bp | 0.52 | 0.62 |
| Heart, VS, ap | 0.81 | 0.83 |
| Heart, RV | 0.56 | 0.73 |

| Reproductive system | Mean | SD |
|---|---|---|
| Prostate | 0.99 | 1.37 |
| Testicle | 1.07 | 1.07 |
| Ovary | bdl | 0.00 |
| Uterus | 1.20 | 1.10 |

| Hematological tissues | Mean | SD |
|---|---|---|
| Blood | 0.69 | 1.38 |
| Bone marrow | 0.98 | 1.28 |

| Urinary tract | Mean | SD |
|---|---|---|
| Right kidney | 0.65 | 0.90 |
| Left kidney | 1.09 | 1.51 |
| Urinary bladder | 0.87 | 1.13 |

Figure 1b

## Respiratory system

| | Patient 1 | Patient 2 | Patient 3 | Patient 4 | Patient 5 | Patient 6 | Patient 7 | Patient 8 | Patient 9 | Patient 10 | Patient 11 |
|---|---|---|---|---|---|---|---|---|---|---|---|
| Mesopharynx | nd | nd | nd | 2.85 | 3.02 | bdl | bdl | 3.00 | 4.45 | 3.15 | bdl |
| Epiglottis | 2.50 | 1.18 | 1.66 | 3.14 | 2.60 | bdl | 2.82 | 2.10 | 4.45 | 3.05 | bdl |
| Trachea middle | 2.46 | 1.36 | 3.03 | 5.27 | 5.47 | bdl | bdl | 3.01 | 5.09 | 2.71 | 1.82 |
| Tracheal bifurcation | 3.01 | 1.13 | 3.28 | 4.82 | 4.98 | bdl | bdl | 3.79 | 4.46 | 2.52 | 1.33 |
| Right lung, UL | 6.17 | bdl | 4.97 | 4.65 | 7.63 | 2.90 | 3.15 | 4.91 | 4.52 | 2.14 | bdl |
| Right lung, ML | 6.82 | 0.88 | 6.08 | 4.64 | 7.61 | 2.17 | 3.06 | 5.40 | 4.26 | 3.01 | bdl |
| Right lung, LL | 6.14 | 3.56 | 4.25 | 4.62 | 7.71 | 1.64 | 3.90 | 4.46 | 4.55 | 3.40 | bdl |
| Left lung, UL | 6.29 | bdl | 6.39 | 5.79 | 7.19 | 4.16 | 3.26 | 5.40 | 4.82 | 3.91 | bdl |
| Left lung, LL | 6.20 | 2.52 | 5.90 | 4.84 | 6.94 | 2.68 | 2.96 | 4.63 | 4.34 | 4.06 | bdl |

## Lymphatic system

| | Patient 1 | Patient 2 | Patient 3 | Patient 4 | Patient 5 | Patient 6 | Patient 7 | Patient 8 | Patient 9 | Patient 10 | Patient 11 |
|---|---|---|---|---|---|---|---|---|---|---|---|
| Tonsilla palatina | nd | nd | nd | 4.16 | 2.45 | np | bdl | 0.81 | 4.03 | 2.64 | bdl |
| Cervical lymph nodes | 0.79 | 2.58 | 2.57 | 3.20 | 5.23 | 2.78 | 1.48 | 2.96 | 3.78 | 2.22 | bdl |
| Hilar lymph nodes | 4.48 | 2.05 | 3.47 | 3.28 | 5.10 | 3.86 | 1.28 | 3.30 | 4.35 | 2.59 | bdl |
| Paraaort. lymph nodes | 1.17 | bdl | 3.82 | 1.55 | 2.78 | np | bdl | 2.99 | 3.56 | bdl | bdl |
| Spleen | 1.68 | bdl | 0.61 | 1.01 | 2.62 | bdl | bdl | bdl | 2.02 | bdl | bdl |
| Appendix vermiformis | 1.03 | bdl | 2.93 | 2.23 | 1.73 | bdl | bdl | bdl | bdl | bdl | bdl |

## Cardiovascular system

| | Patient 1 | Patient 2 | Patient 3 | Patient 4 | Patient 5 | Patient 6 | Patient 7 | Patient 8 | Patient 9 | Patient 10 | Patient 11 |
|---|---|---|---|---|---|---|---|---|---|---|---|
| Aortic arch | 2.41 | bdl | 3.00 | 3.51 | 3.55 | bdl | bdl | 0.99 | 3.32 | bdl | bdl |
| Pulmonary artery | nd | nd | nd | 3.47 | 5.73 | 1.68 | bdl | 3.67 | 4.43 | 2.52 | bdl |
| Abdominal aorta, sr | 1.47 | bdl | 0.00 | 1.77 | 3.05 | bdl | bdl | 0.80 | 3.50 | 2.15 | 0.73 |
| Heart, LV, aw, pb | 2.49 | bdl | 0.86 | 0.66 | 2.00 | bdl | bdl | 0.83 | 2.58 | bdl | bdl |
| Heart, LV, aw, ap | 2.10 | bdl | 0.46 | 0.00 | 1.94 | bdl | bdl | 0.77 | 1.37 | 1.82 | bdl |
| Heart, LV, pw, bp | 1.73 | bdl | 0.84 | 0.46 | 1.24 | bdl | bdl | 0.83 | 0.77 | bdl | bdl |
| Heart, LV, pw, ap | 1.60 | bdl | 1.02 | 0.67 | 2.58 | bdl | bdl | 1.11 | 1.11 | bdl | bdl |
| Heart, VS, bp | 0.96 | bdl | 1.48 | 0.00 | 1.42 | bdl | bdl | 0.81 | 1.00 | bdl | bdl |
| Heart, VS, ap | 0.91 | bdl | 1.09 | 0.00 | 2.08 | bdl | bdl | 1.41 | 1.59 | 1.80 | bdl |
| Heart, RV | 0.93 | bdl | 1.08 | 0.72 | 2.12 | bdl | bdl | 1.30 | bdl | bdl | bdl |

## Hematological tissues

| | Patient 1 | Patient 2 | Patient 3 | Patient 4 | Patient 5 | Patient 6 | Patient 7 | Patient 8 | Patient 9 | Patient 10 | Patient 11 |
|---|---|---|---|---|---|---|---|---|---|---|---|
| Blood | bdl | bdl | 3.20 | 1.14 | 3.89 | bdl | bdl | bdl | bdl | bdl | bdl |
| Bone marrow | 0.92 | bdl | 0.74 | 2.06 | 2.82 | bdl | bdl | 1.50 | 3.69 | bdl | bdl |

| *SARS-CoV-2 RNA in log10* |
|---|
| *bdl* |
| *0.01 – 0.99* |
| *1.00 – 1.99* |
| *2.00 – 2.99* |
| *3.00 – 3.99* |
| *from 4.00* |

Figure 1c

## Gastrointestinal tract

| | Patient 1 | Patient 2 | Patient 3 | Patient 4 | Patient 5 | Patient 6 | Patient 7 | Patient 8 | Patient 9 | Patient 10 | Patient 11 |
|---|---|---|---|---|---|---|---|---|---|---|---|
| Tongue | nd | nd | nd | 3.06 | 2.30 | bdl | bdl | 1.30 | 3.53 | 3.12 | bdl |
| Gl. submandibularis | nd | nd | nd | 1.24 | 1.56 | bdl | bdl | bdl | 1.85 | 1.78 | 1.06 |
| Oesophagus | nd | nd | nd | 2.01 | 2.82 | bdl | bdl | 1.59 | 4.04 | 2.51 | bdl |
| Stomach, corpus | 1.57 | bdl | 0.81 | bdl | 1.39 | bdl | bdl | bdl | 6.24 | bdl | bdl |
| Duodenum | 2.13 | bdl | 1.29 | 1.39 | bdl | bdl | bdl | bdl | 4.92 | bdl | bdl |
| Jejunum | 0.89 | bdl | 2.25 | 2.22 | 1.25 | bdl | bdl | bdl | 4.43 | bdl | bdl |
| Pancreas | bdl | bdl | bdl | bdl | bdl | bdl | bdl | bdl | 1.84 | bdl | 0.83 |
| Liver | bdl | bdl | 1.90 | 1.19 | 2.29 | bdl | bdl | 0.70 | bdl | 2.31 | bdl |
| Gall bladder | bdl | bdl | 2.14 | bdl | bdl | bdl | bdl | bdl | 0.79 | bdl | 1.04 |
| Ileum | bdl | bdl | 4.72 | 1.37 | 1.70 | bdl | bdl | bdl | 4.76 | 2.20 | bdl |
| Colon | bdl | bdl | 4.80 | 0.74 | 1.32 | bdl | bdl | bdl | 4.45 | bdl | bdl |
| Rectum | bdl | bdl | 2.30 | bdl | 1.92 | bdl | bdl | 0.84 | 2.35 | 2.01 | bdl |

## Endocrine system

| | Patient 1 | Patient 2 | Patient 3 | Patient 4 | Patient 5 | Patient 6 | Patient 7 | Patient 8 | Patient 9 | Patient 10 | Patient 11 |
|---|---|---|---|---|---|---|---|---|---|---|---|
| Thyroid gland | bdl | bdl | 2.76 | 2.38 | 3.56 | bdl | bdl | 2.39 | 4.10 | 2.44 | bdl |
| Adrenal gland | bdl | bdl | bdl | 2.16 | 2.17 | bdl | bdl | 0.57 | 2.58 | 1.62 | bdl |

## Urinary tract

| | Patient 1 | Patient 2 | Patient 3 | Patient 4 | Patient 5 | Patient 6 | Patient 7 | Patient 8 | Patient 9 | Patient 10 | Patient 11 |
|---|---|---|---|---|---|---|---|---|---|---|---|
| Right kidney | bdl | bdl | 0.61 | 1.18 | 2.32 | bdl | bdl | 0.84 | 2.22 | bdl | bdl |
| Left kidney | bdl | bdl | 1.58 | 1.11 | 4.42 | bdl | bdl | bdl | 2.95 | 1.98 | bdl |
| Urinary bladder | 0.96 | bdl | 1.30 | 0.97 | 1.90 | bdl | bdl | bdl | 3.65 | bdl | 0.81 |

## Nervous system

| | Patient 1 | Patient 2 | Patient 3 | Patient 4 | Patient 5 | Patient 6 | Patient 7 | Patient 8 | Patient 9 | Patient 10 | Patient 11 |
|---|---|---|---|---|---|---|---|---|---|---|---|
| Brain, frontal lobe | bdl | bdl | 2.15 | 0.47 | 1.77 | bdl | bdl | bdl | bdl | bdl | bdl |
| Brain, hippocampus | bdl | bdl | 1.65 | 1.26 | 1.41 | bdl | bdl | bdl | bdl | bdl | bdl |
| Cerebellum | bdl | bdl | 0.00 | 2.06 | 2.01 | bdl | bdl | bdl | bdl | bdl | bdl |
| Brain stem, pons | bdl | bdl | 3.96 | 2.05 | 1.60 | bdl | bdl | bdl | bdl | bdl | bdl |
| N. phrenicus | nd | nd | nd | nd | nd | bdl | bdl | 0.82 | 2,56 | bdl | bdl |

## Reproductive system

| | Patient 1 | Patient 2 | Patient 3 | Patient 4 | Patient 5 | Patient 6 | Patient 7 | Patient 8 | Patient 9 | Patient 10 | Patient 11 |
|---|---|---|---|---|---|---|---|---|---|---|---|
| Prostate | bdl | bdl | 3.49 | 1.86 | 1.58 | bdl | bdl | np | np | np | np |
| Testicle | 1.56 | bdl | 1.31 | 2.27 | 2.37 | bdl | bdl | np | np | np | np |
| Ovary | np | np | np | np | np | np | np | bdl | bdl | bdl | bdl |
| Uterus | np | np | np | np | np | np | np | bdl | 2.46 | 1.70 | 0.63 |

| *SARS-CoV-2 RNA in log10* |
|---|
| *bdl* |
| *0.01 – 0.99* |
| *1.00 – 1.99* |
| *2.00 – 2.99* |
| *3.00 – 3.99* |
| *from 4.00* |

# Figure 2

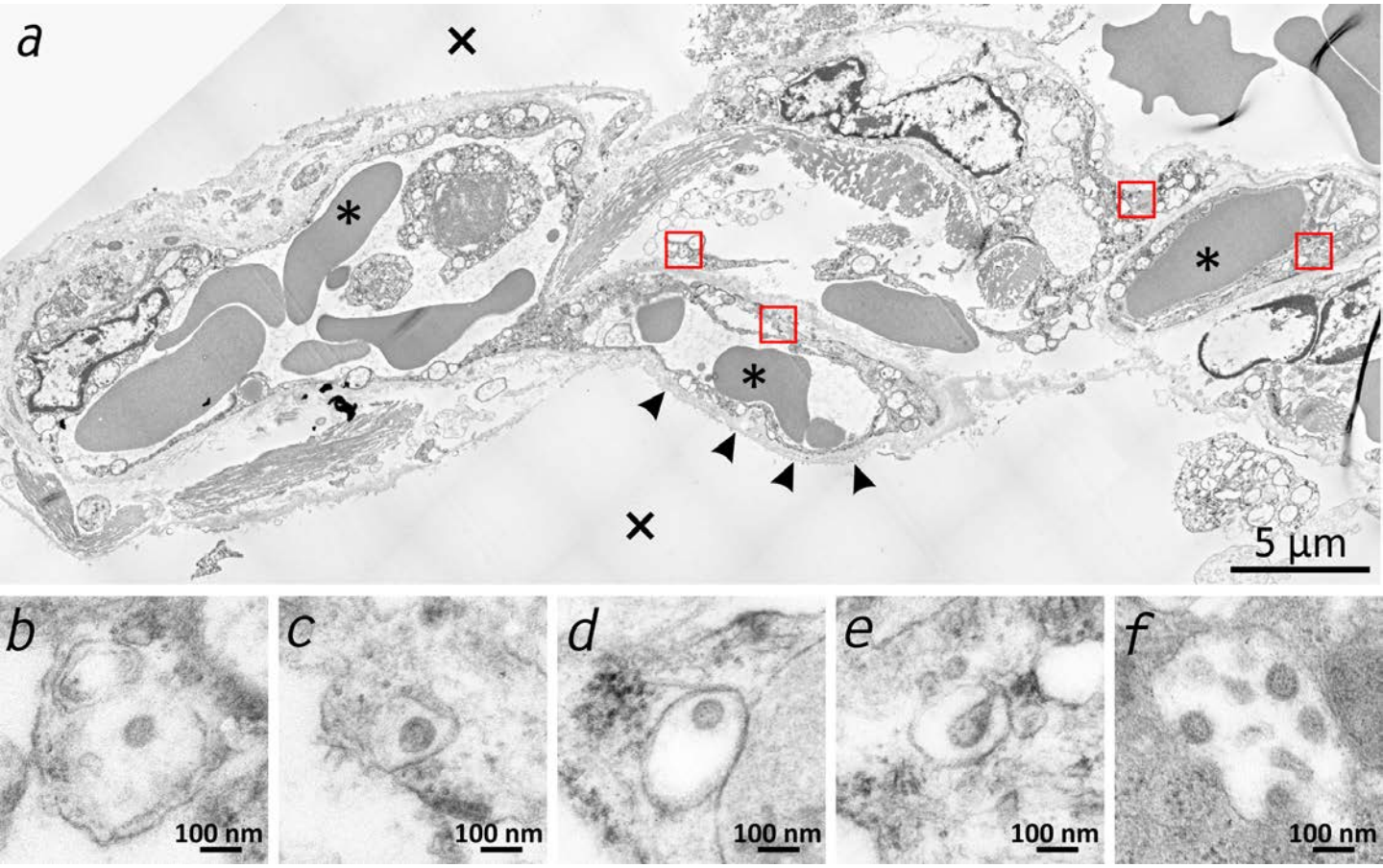

Figure 3

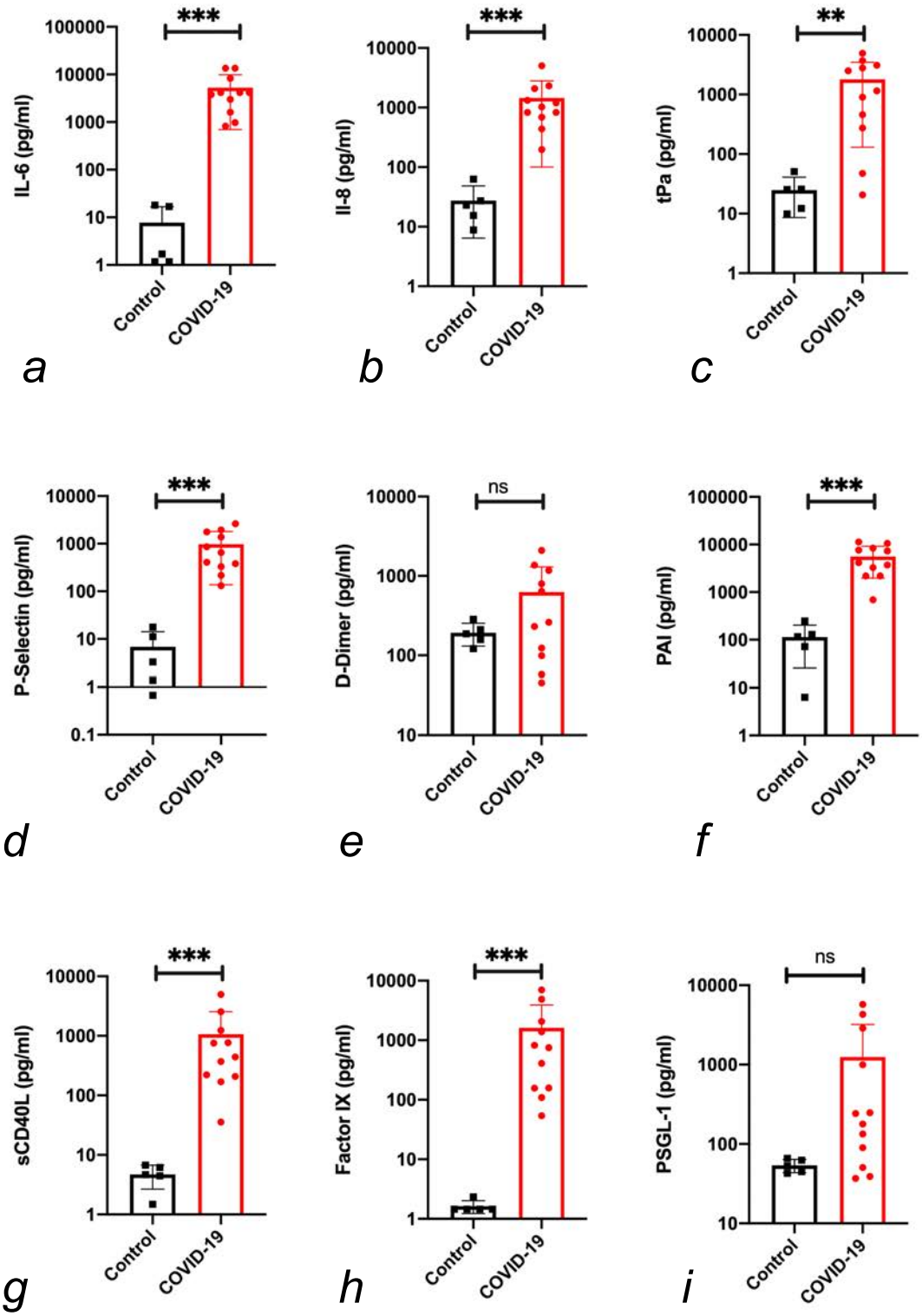
IL-6 (pg/ml)
***
100000
10000
1000
100
10
1
Control
COVID-19
a
Il-8 (pg/ml)
***
10000
1000
100
10
1
Control
COVID-19
b
tPa (pg/ml)
**
10000
1000
100
10
1
Control
COVID-19
c
P-Selectin (pg/ml)
***
10000
1000
100
10
1
0.1
Control
COVID-19
d
D-Dimer (pg/ml)
ns
10000
1000
100
10
Control
COVID-19
e
PAI (pg/ml)
***
100000
10000
1000
100
10
1
Control
COVID-19
f
sCD40L (pg/ml)
***
10000
1000
100
10
1
Control
COVID-19
g
Factor IX (pg/ml)
***
10000
1000
100
10
1
Control
COVID-19
h
PSGL-1 (pg/ml)
ns
10000
1000
100
10
Control
COVID-19
i

# Figure 4

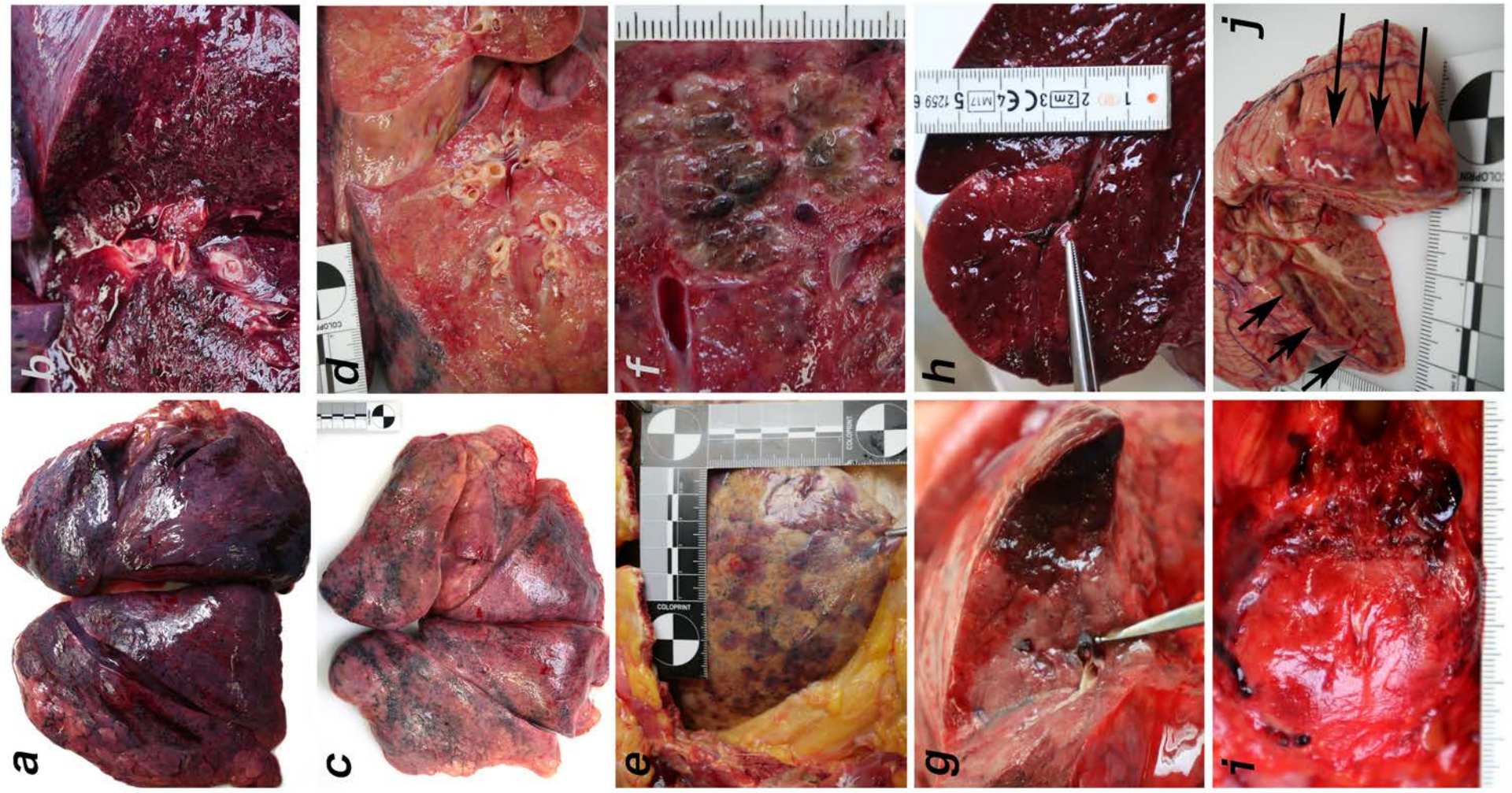

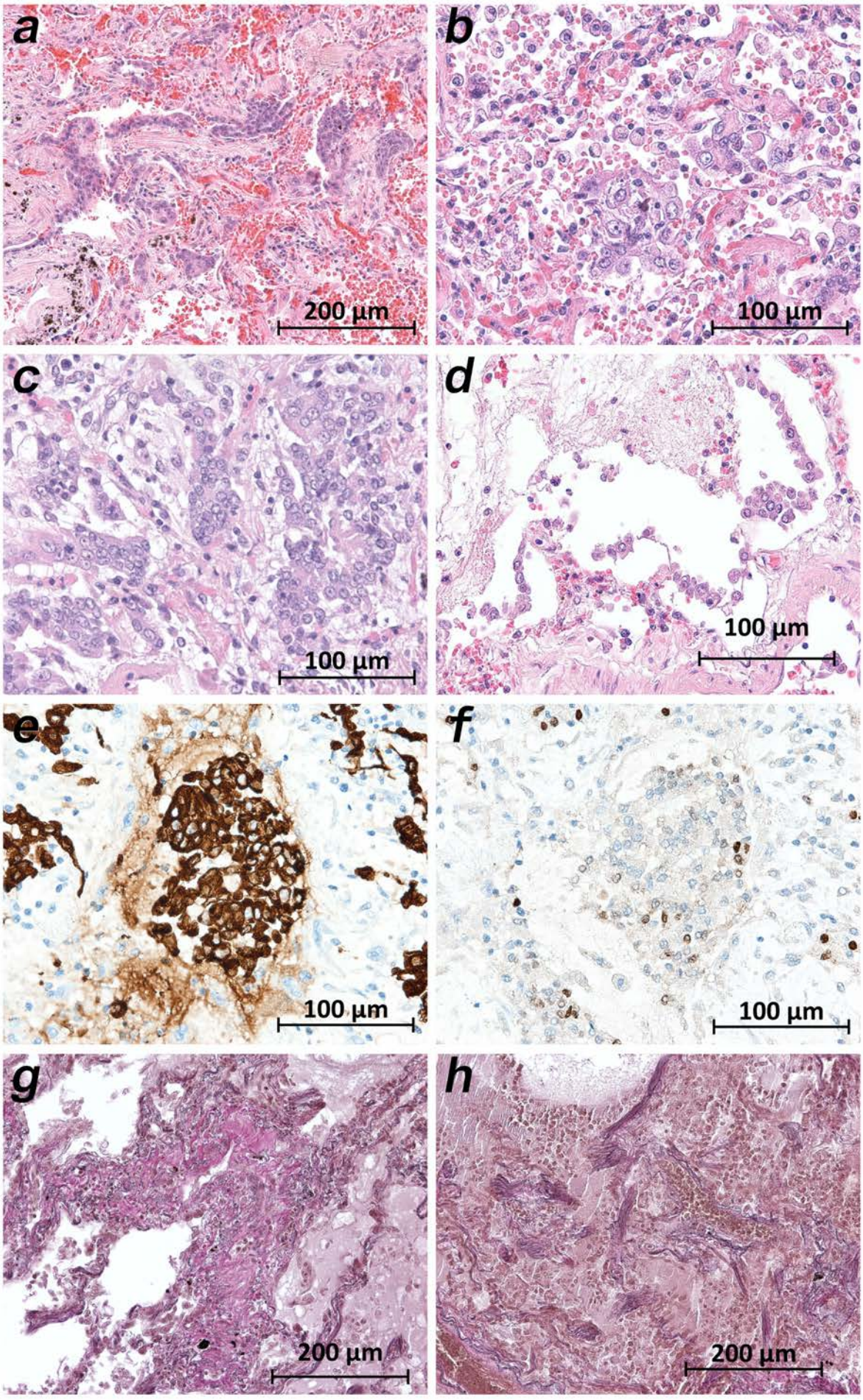


Figure 5

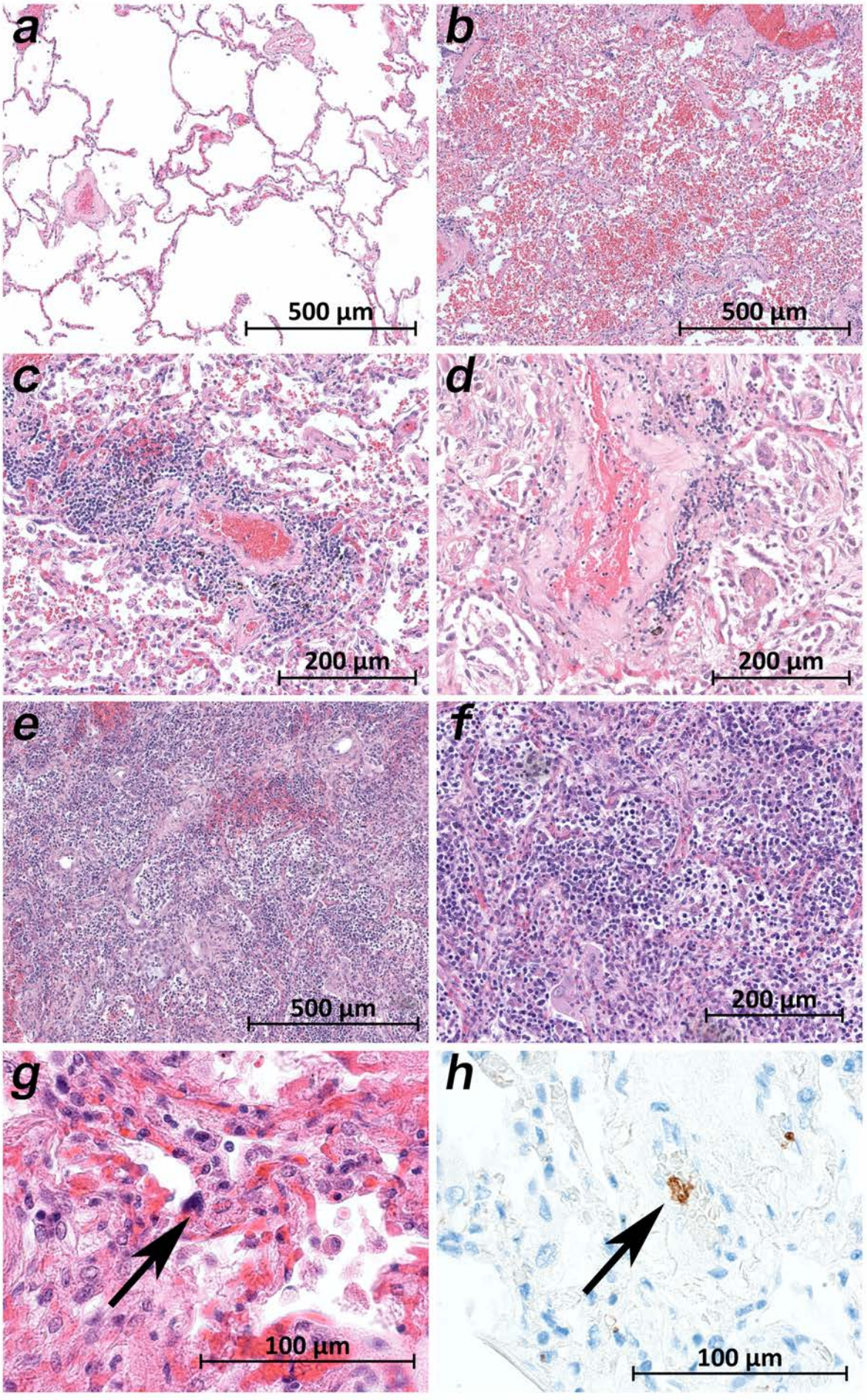


Figure 6

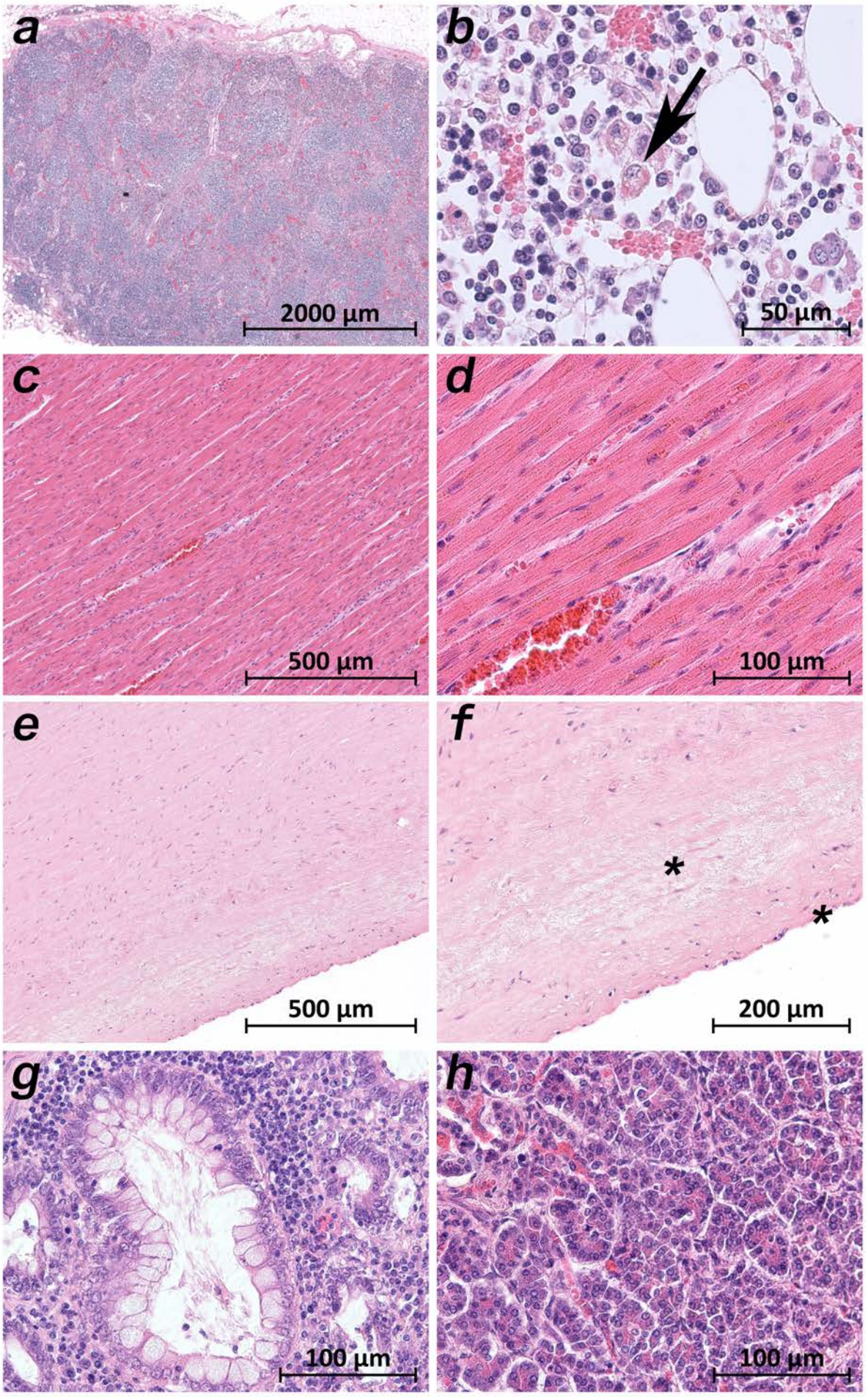


Figure 7

# Early postmortem mapping of SARS-CoV-2 RNA in patients with COVID-19 and correlation to tissue damage

Tables

# Table 1

| | patient 1 | patient 2 | patient 3 | patient 4 | patient 5 | patient 6 | patient 7 | patient 8 | patient 9 | patient 10 | patient 11 |
|---|---|---|---|---|---|---|---|---|---|---|---|
| **sex** | m | m | m | m | m | m | m | f | f | f | f |
| **age [years]** | 82 | 66 | 78 | 54 | 80 | 64 | 64 | 87 | 83 | 85 | 52 |
| **BMI [kg/m²]** | 23.8 | 31.5 | 25.2 | 28.3 | 28.8 | 35.4 | 24.6 | 24.6 | 28.9 | 26.2 | 21.4 |
| **pre-existing medical conditions** | AF, DM, autoimmune pancreatitis, purpura pigmentosa | aHT | aHT, DM, CRF, PAD, urosepsis shortly before COVID-19 | none known | DM, CRF, CHF | GPA, CRF, COPD, aHT, AF, DM | AS, COPD | CHF, CRF, DM, past stroke epilepsy, erysipelas shortly before COVID-19 | aHT, DM, CRF, 1-vessel-CHD, AF, PAD | CHF, CRF, DM | cervical carcinoma |
| **hospitalization [d]** | 7 | 5 | 30 | 10 | 9 | 20 | 15 | 12 | 7 | 9 | 4 |
| **ICU [d]** | 7 | 5 | 7 | 8 | 8 | 17 | 9 | 0 | 0 | 0 | 4 |
| **mechanical ventilation [d]** | 7 | 4 | 7 | 7 | 8 | 16 | 9 (ECMO) | 0 | 0 | 0 | 0 |
| **virustatic medication** | lopinavir, ritonavir | lopinavir, ritonavir | none | none | none | lopinavir, ritonavir | lopinavir, ritonavir | none | none | none | none |
| **cause of death (acc. to clinic)** | MOF | pulmonary embolism | MOF | lung failure | suspected myocardial infarction | lung failure | lung failure | respiratory failure | pneumonia | pneumonia | ileus |

**Table 1 Clinical characteristics of the patients.**

Abbreviations:
aHT – arterial hypertension
AF – atrial fibrillation
AS – atherosclerosis
CHF – chronic heart failure
CHD – coronary heart disease
COPD – chronic obstructive pulmonary disease
CRF – chronic renal failure
DM – diabetes mellitus
f – female
GPA – granulomatosis with polyangiitis (Wegener's Granulomatosis)
ICU – intensive care unit
MOF – multiple organ failure
PAD – peripheral artery disease

| | | patient 1 | patient 2 | patient 3 | patient 4 | patient 5 | patient 6 | patient 7 | patient 8 | patient 9 | patient 10 | patient 11 |
|---|---|---|---|---|---|---|---|---|---|---|---|---|
| **PMI [h]** | | 3.5 | 2.25 | 7.5 | 9.5 | 15.0 | 2.33 | 1.5 | 5.8 | 5.0 | 6.0 | 3.5 |
| **lung weight** | | R 1550 g<br>L 1240 g | R 940 g<br>L 760 g | R 1170 g<br>L 790 g | R 1860 g<br>L 1640 g | R 1370 g<br>L 990 g | R 970 g<br>L 570 g | R 890 g<br>L 770 g | R 610 g<br>L 480 g | R 550 g<br>L 680 g | R 530 g<br>L 400 g | R 760 g<br>L 590 g |
| **lung macro*** | **edema** | +++ | ++ | ++ | ++ | ++ | + | + | + | + | ++ | + |
| | **hypermia** | +++ | + | +++ | ++ | ++ | + | + | + | + | ++ | + |
| | **hemorrhage** | +++ | + | +++ | ++ | ++ | ++ | + | - | + | ++ | + |
| | **texture** | reduced | reduced | reduced | reduced | reduced | enhanced | enhanced | enhanced | reduced | reduced | reduced |
| | **infarction** | - | - | + | + | - | - | - | - | - | - | - |
| **lung micro*** | **DAD, exsudative phase** | +++ | ++ | ++ | ++ | +++ | + | + | + | + | ++ | + |
| | **DAD, proliferative phase** | ++ | - | - | + | + | +++ | +++ | +++ | ++ | ++ | - |
| | **multinucleated giant cells** | +++ | ++ | ++ | ++ | ++ | + | + | - | ++ | + | + |
| | **squamous metaplasia** | +++ | + | ++ | ++ | ++ | + | ++ | ++ | ++ | +++ | + |
| | **megakaryocytes** | - | - | - | - | - | + | + | ++ | + | - | + |
| | **lymphocytic infiltrates** | + | + | - | - | ++ | - | +++ | - | - | + | - |
| | **vasculitis** | - | + | + | + | - | - | - | + | + | - | - |
| | **stasis / fibrin thrombi** | + | + | - | - | - | - | - | + | + | + | tumor |
| | **emboli** | - | ++ | - | + | + | - | - | - | - | + | tumor |
| | **superinfection** | - | - | fungal | - | - | bacterial | - | - | bacterial | bacterial | - |
| **heart weight** | | 480 g | 600 g | 550 g | 430 g | 810 g | 610 g | 480 g | 380 g | 360 g | 300 g | 350 g |
| **heart macro** | | pericarditis, 2-v-CHD | conc. HT | 3-v-CHD | un-remarkable | exc. HT | exc. HT | - | 2-v-CHD | 3-v-CHD | 1-v-CHD | un-remarkable |
| **heart micro** | | moderate fibrosis | moderate fibrosis | chronic ischemia | un-remarkable | amyloidosis | slight fibrosis | slight fibrosis | slight fibrosis | moderate fibrosis | atrophy, fibrosis | invasive metastases |
| **further autopsy findings (besides age-related or pre-existing)** | | steatosis hepatis | NASH | - | CLL, ICH, spleen infarction | severe cardiac amyloidosis | hepatic siderosis | - | adrenal thrombosis | - | endometrial carcinoma (apT1a) | cervical carcinoma (apT4) |
| **cause of death (acc. to autopsy) **** | | COVID-19 (HP) | COVID-19 (pulmonary embolism) | COVID-19 (HP) | COVID-19 (HP) | COVID-19 (HP) | COVID-19 (CCP) | COVID-19 (CCP) | COVID-19 (CCP) | COVID-19 (BP+HP) | COVID-19 (BP+HP) | malignant tumor disease |

**Table 2 Autopsy findings.**

Abbreviations:
BP – bronchopneumonia
CCP – chronic carnifying pneumonia
CHD – coronary heart disease
CLL – chronic lymphatic leukemia
DAD – diffuse alveolar damage
HP – hemorrhagic pneumonia
HT – hypertrophy, conc. = concentric, exc. = excentric
ICH – intracerebral hemorrhage
NASH – non-alcoholic steatosis hepatitis
PMI – postmortem interval (time between death and autopsy)
v – vessel

* Semi-quantitative evaluation: no (-), few (+), moderate (++), very much (+++)
** Supplemented term within brackets describes the dominant finding that caused death by COVID-19.

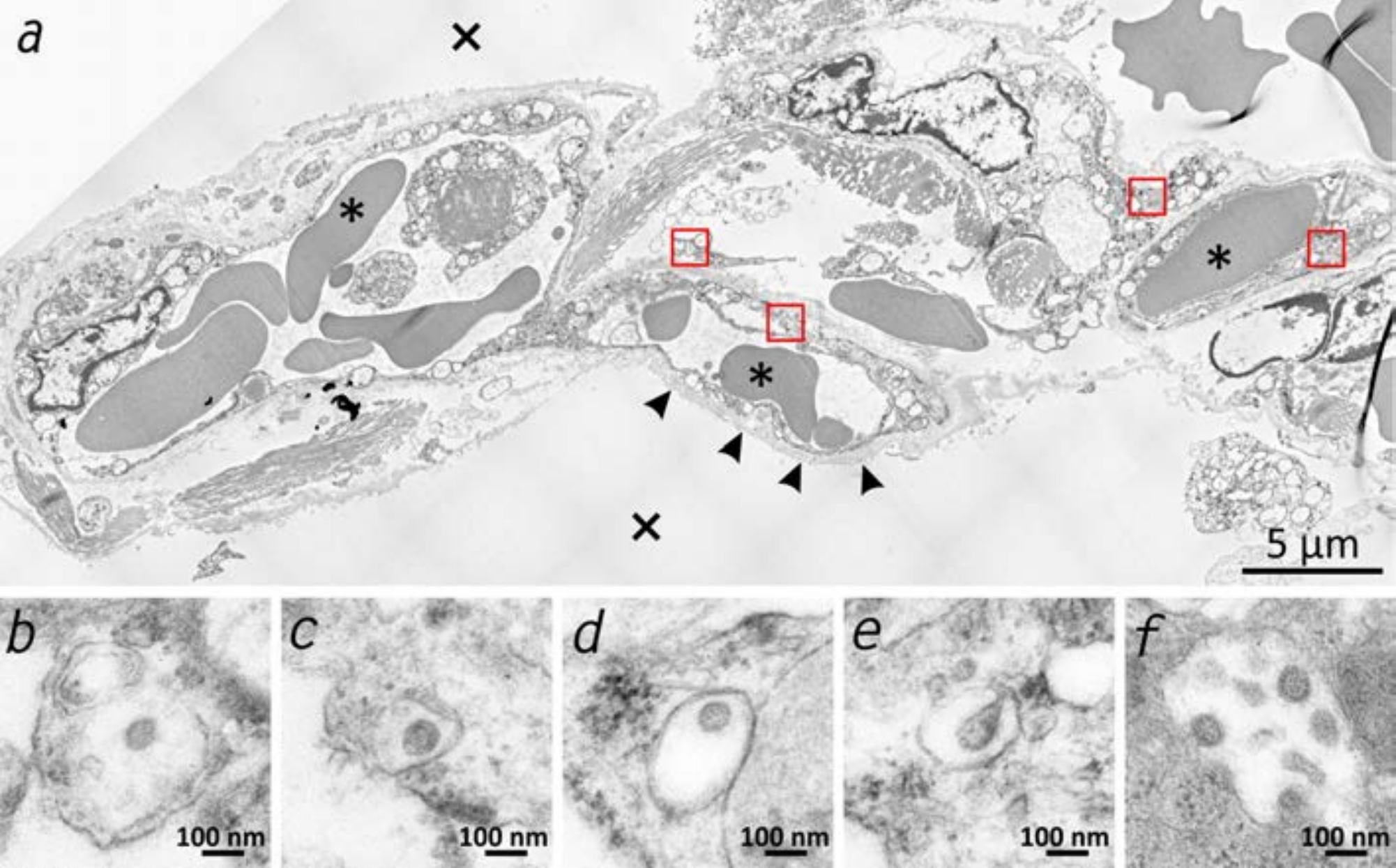
a
5 µm
b
100 nm
c
100 nm
d
100 nm
e
100 nm
f
100 nm

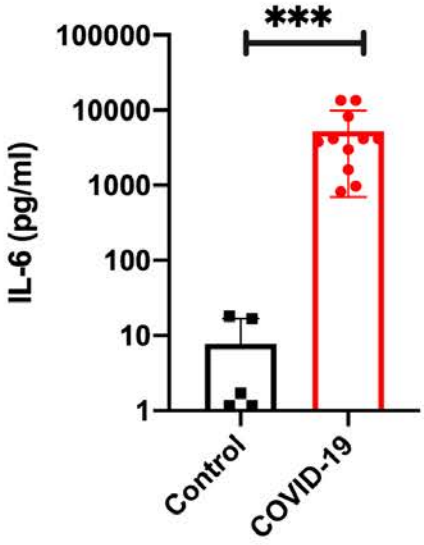
***
IL-6 (pg/ml)
100000
10000
1000
100
10
1
Control
COVID-19

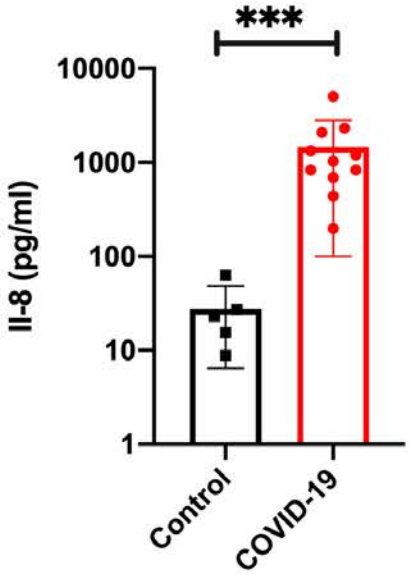
***
Il-8 (pg/ml)
10000
1000
100
10
1
Control
COVID-19

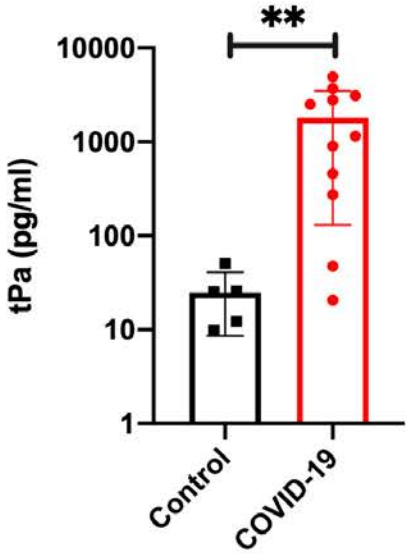
**
tPa (pg/ml)
10000
1000
100
10
1
Control
COVID-19

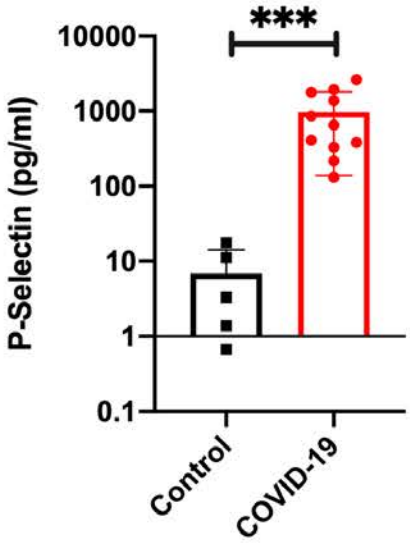
***
P-Selectin (pg/ml)
10000
1000
100
10
1
0.1
Control
COVID-19

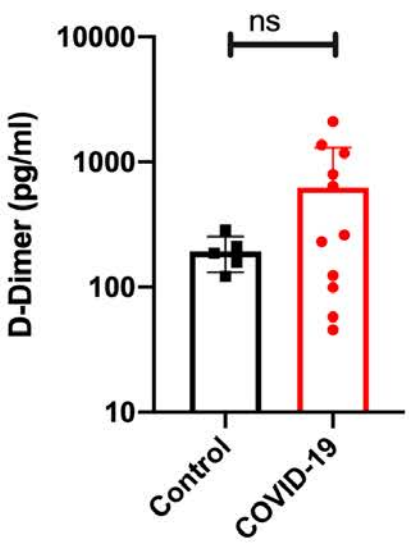
ns
D-Dimer (pg/ml)
10000
1000
100
10
Control
COVID-19

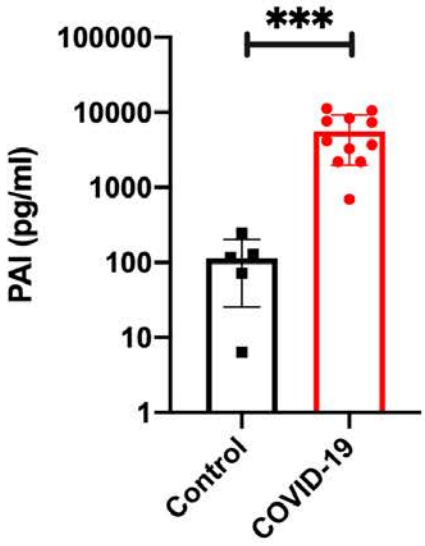
***
PAI (pg/ml)
100000
10000
1000
100
10
1
Control
COVID-19

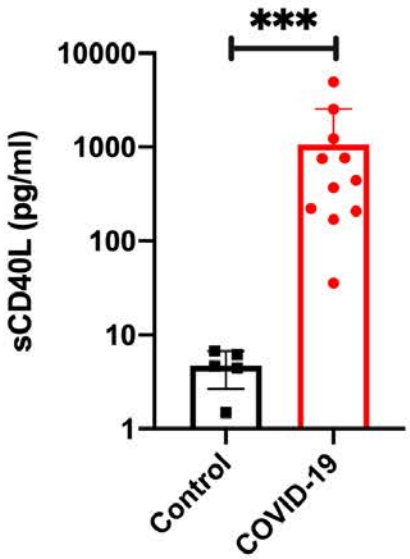
***
sCD40L (pg/ml)
10000
1000
100
10
1
Control
COVID-19

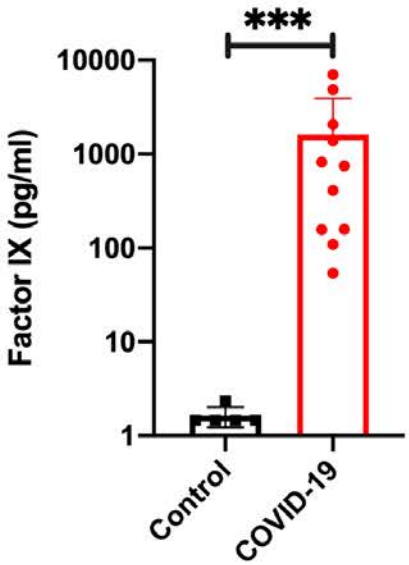
***
Factor IX (pg/ml)
10000
1000
100
10
1
Control
COVID-19

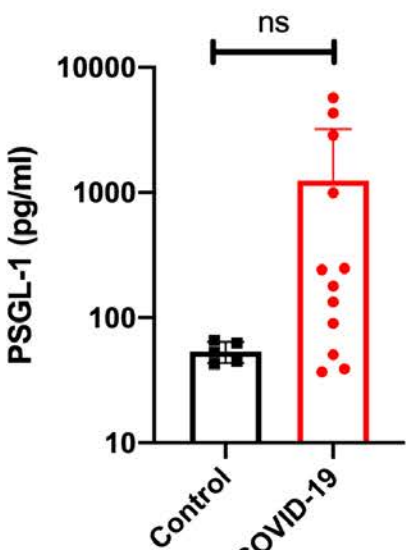
ns
PSGL-1 (pg/ml)
10000
1000
100
10
Control
COVID-19